Nanofab Facility : the Clean Room 500 m2

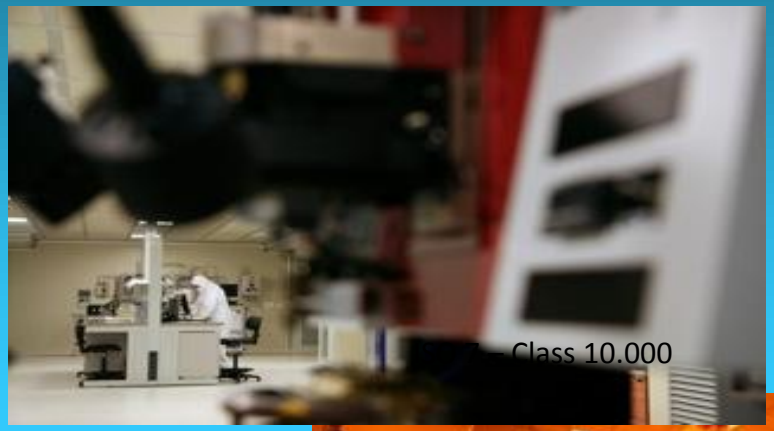

Class 10.000

ISO 6 – Class 1.000
Yellow Room

2D-3D structures

3D PH. Crys. By X-ray litho

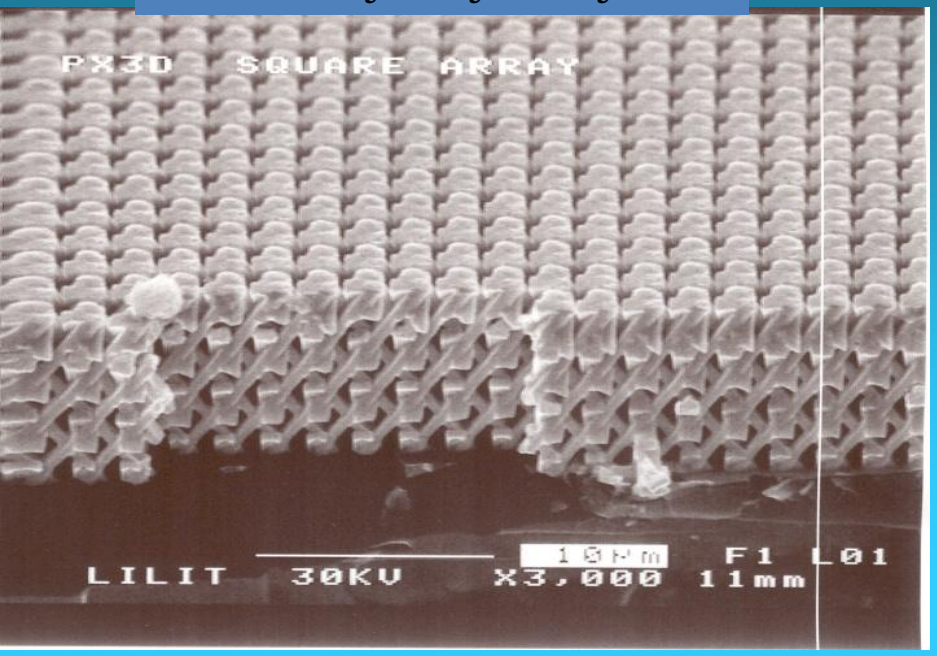

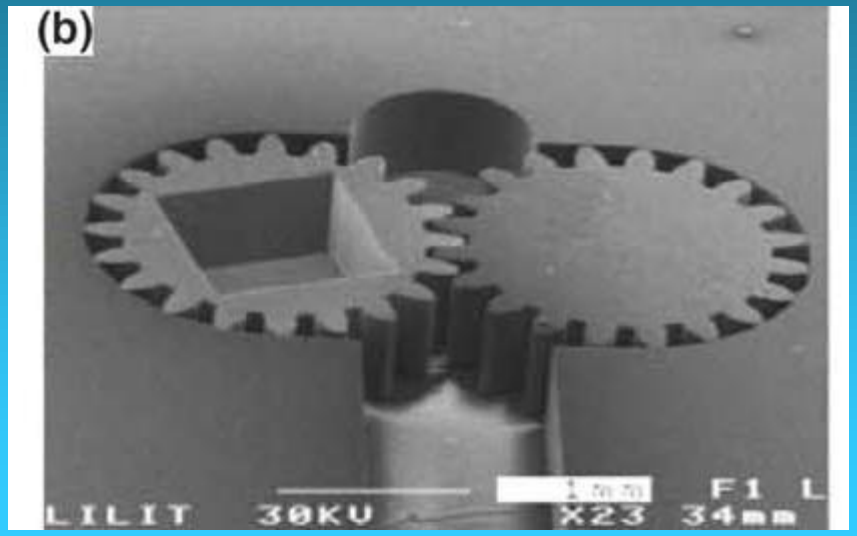

Topographic lenses

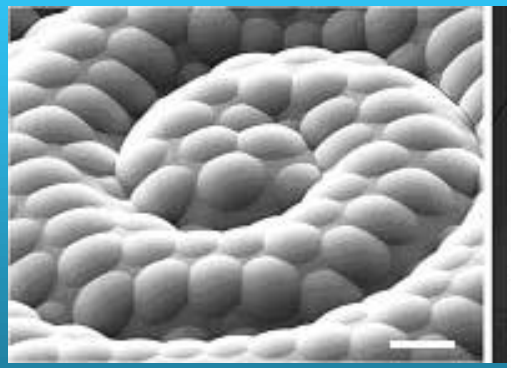

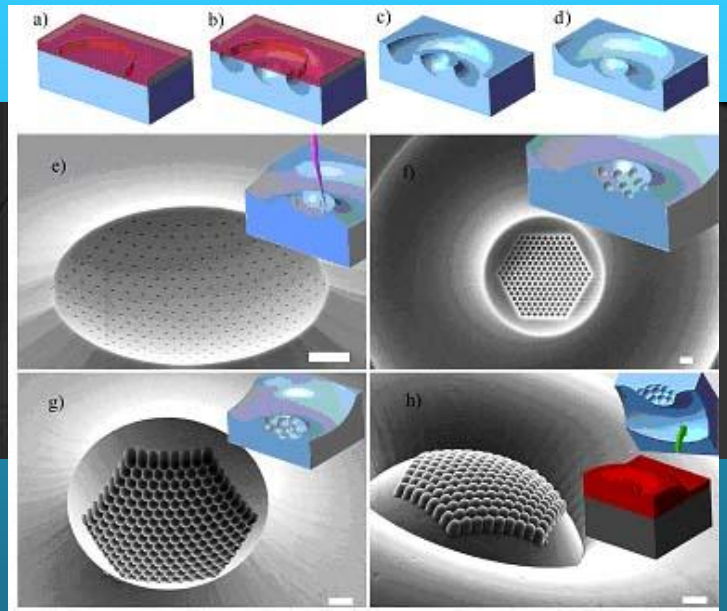

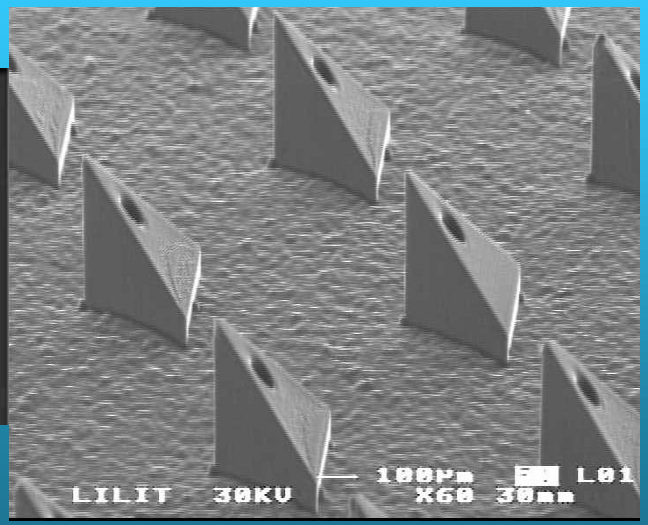

Determining the structure of matter

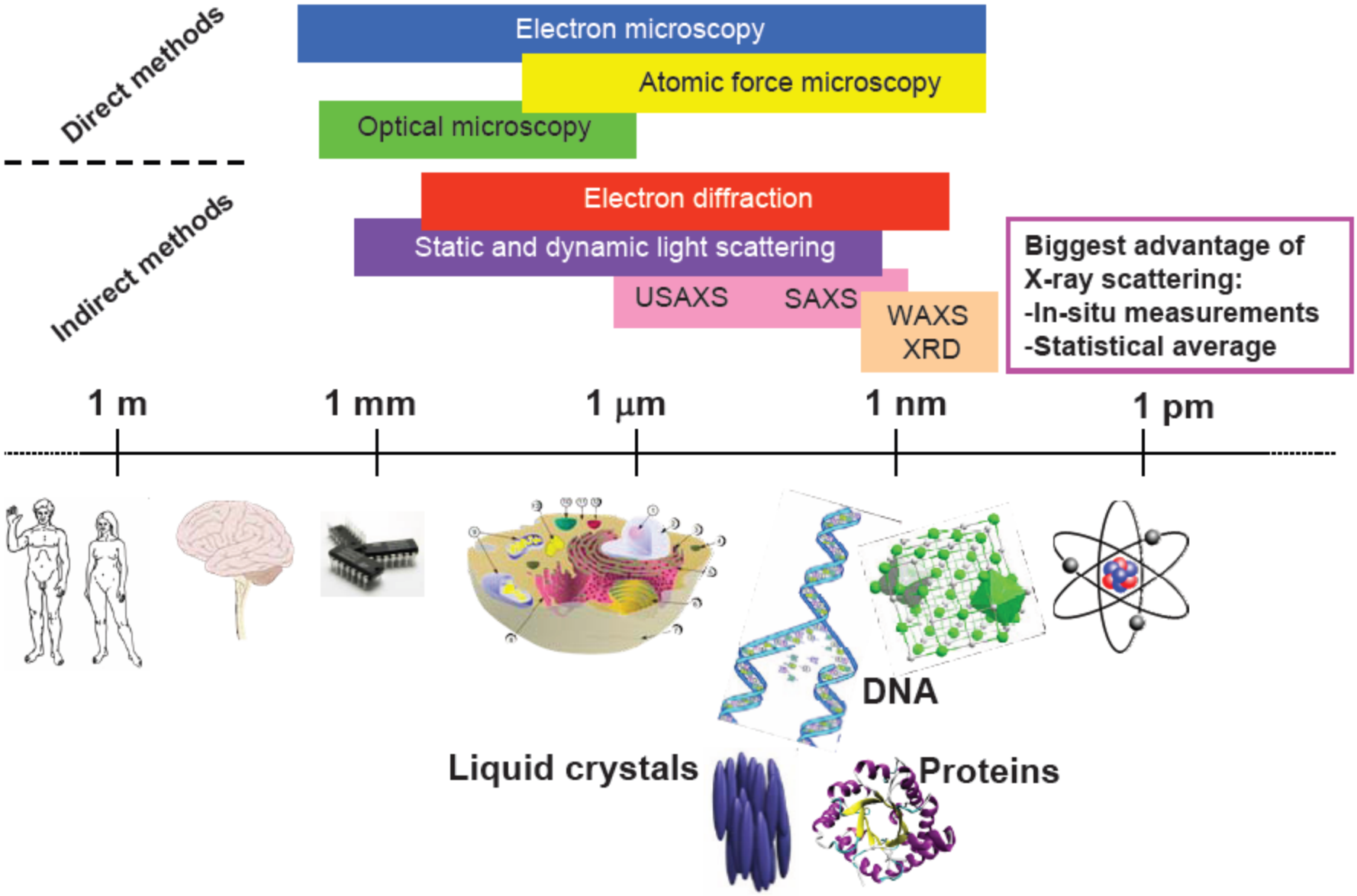

PARAMETER TABLE BEND MAGNET

Parameters *	SuperB HER	SuperB LER	NSLS II	APS	ESRF	ELETTRA	ALS
E [GeV]	6.7	4.18	3	7.0	6.03	2.0	1.9
I [mA]	1892	2447	500	100	200	320	500
ρ [m]	69.64	26.8	24.975	38.961	23.623	5.55	4.81
εx [m rad]	2.0 E-9	2.46 E-9	0.55 E-9	2.514 E-9	4.0 E-9	7.0 E-9	6.3 E-9
εy [m rad]	5.0 E-12	6.15 E-12	8.0 E-12	22.6 E-12	25.0 E-12	70.0 E-12	50 E-12
γy [m^-1]	0.334	0.537	0.05	0.101	0.10	0.5	0.740
σx [mm]	82.1 E-3	92.1 E-3	125.0 E-3	81.7 E-3	77.0 E-3	139.0 E-3	101.8 E-3
σy [mm]	8.66 E-3	9.11 E-3	13.4 E-3	27.0 E-3	29.5 E-3	28.0 E-3	8.2 E-3

* Source of data different web pages, CDRs and presentations

SPECTRAL BRIGHTNESS BEND MAGNET

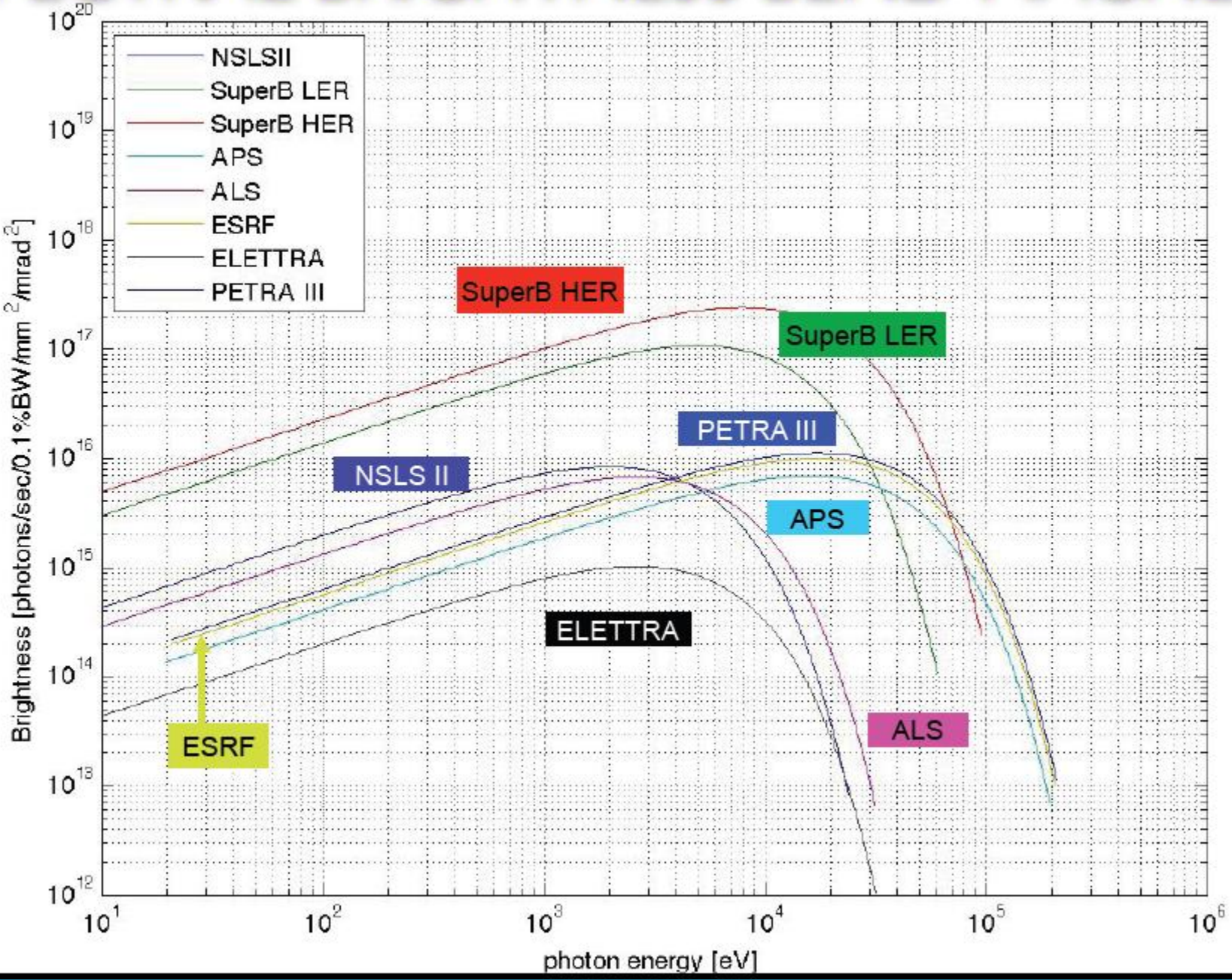

PARAMETER TABLE UNDULATOR

Parameters *	SuperB HER	SuperB LER	NSLS II	APS	PEPX	Soleil	Spring8	Petra III
	IVU20	IVU20	IVU20	U33	IVU23	U20	U24	U29
E [GeV]	6.7	4.18	3	7.0	4.5	2.75	8.0	6.0
I [mA]	1892	2447	500	100	1500	500	100	100
σx [mm]	60.0 E-3	66.5 E-3	33.3 E-3	278 E-3	22.2 E-3	3.88 E-1	286 E-3	140 E-3
σy [mm]	2.4 E-3	2.6 E-3	2.9 E-3	8.9 E-3	7.0 E-3	8.08 E-3	6.0 E-3	5.6 E-3
σx' [mrad]	33.3 E-3	37.0 E-3	16.5 E-3	11.8 E-3	7.4 E-3	14.5 E-3	11.0 E-3	7.9 E-3
σy' [mrad]	2.1 E-3	2.7 E-3	2.7 E-3	3.3 E-3	1.2 E-3	4.6 E-3	1.0 E-3	4.1 E-6
N [1]	148	148	148	72	150	90	186	172
λu [mm]	20	20	20	33	23	20	24	29
Kmax [1]	1.83	1.83	1.83	2.75	2.26	1.0	2.21	2.2
Kmin [1]	0.1	0.1	0.1	0.1	0.1	0.1	0.1	0.1

* Source of data different web pages, CDRs and presentations

SPECTRAL BRIGHTNESS UNDULATOR

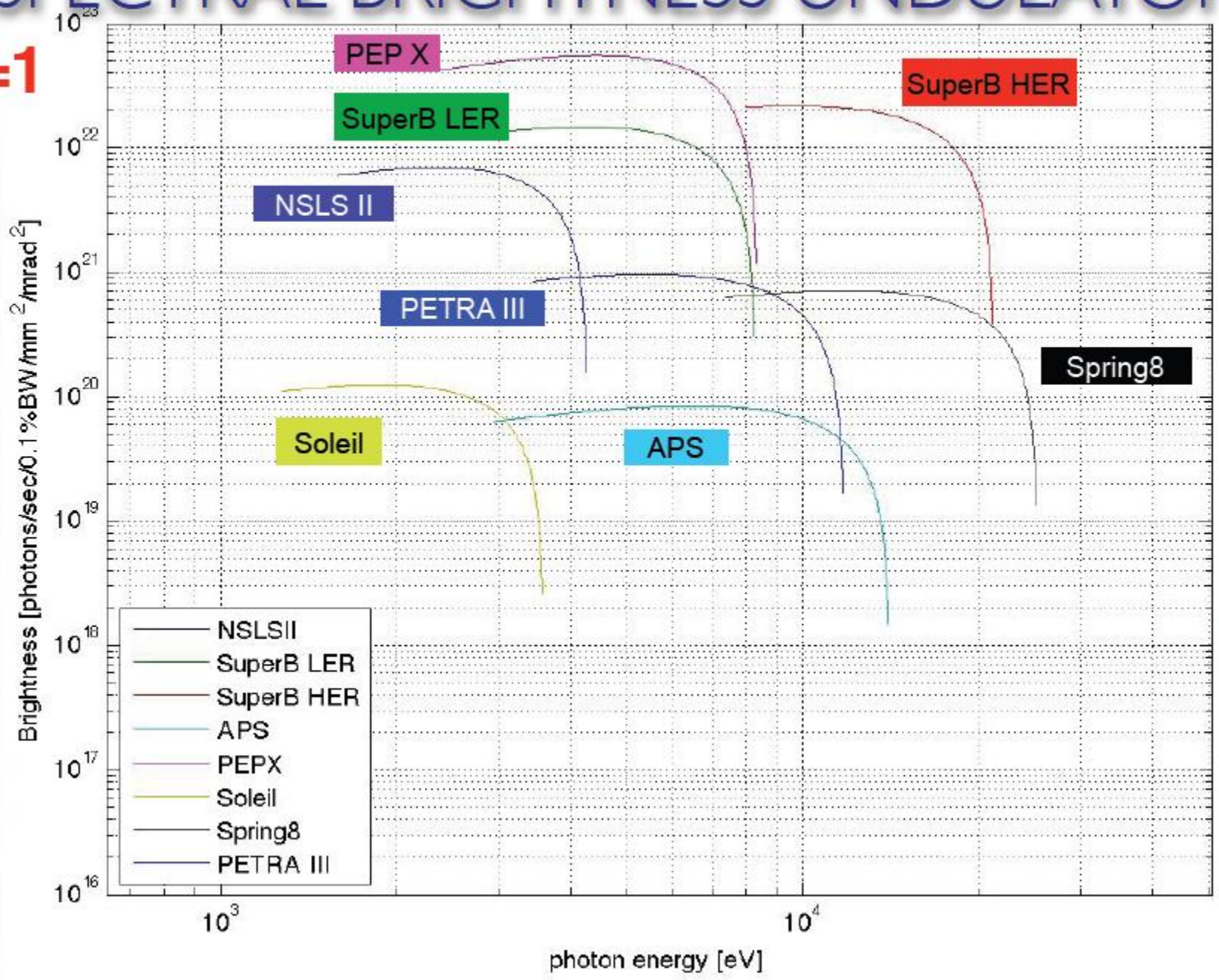

ZPs and DOE: spatial and temporal coherence

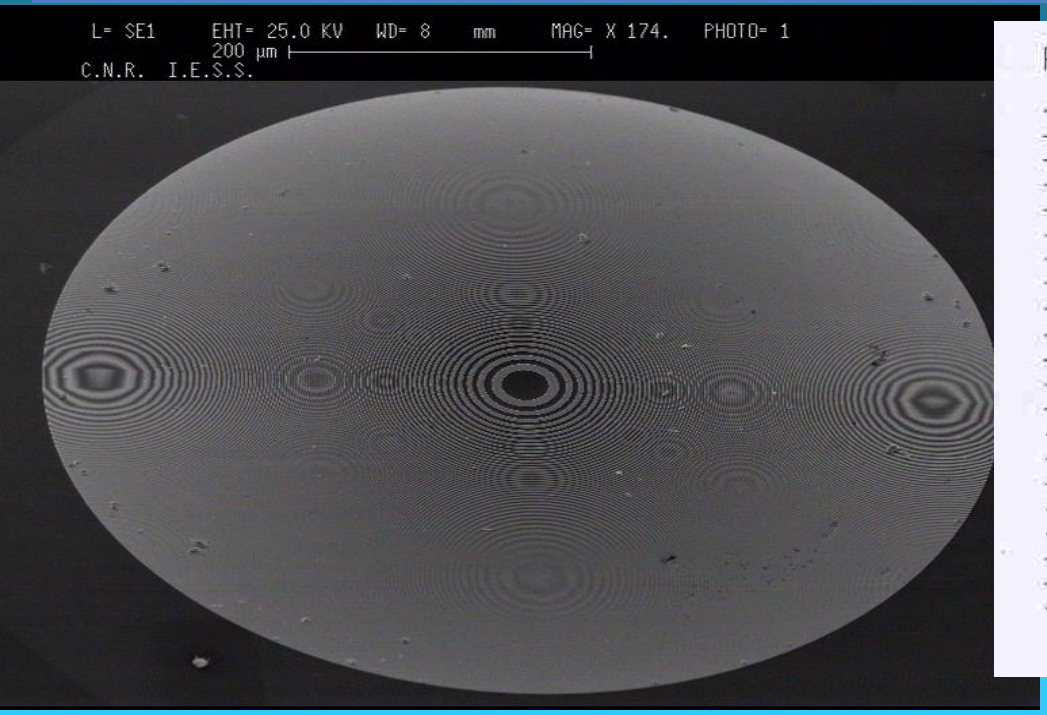

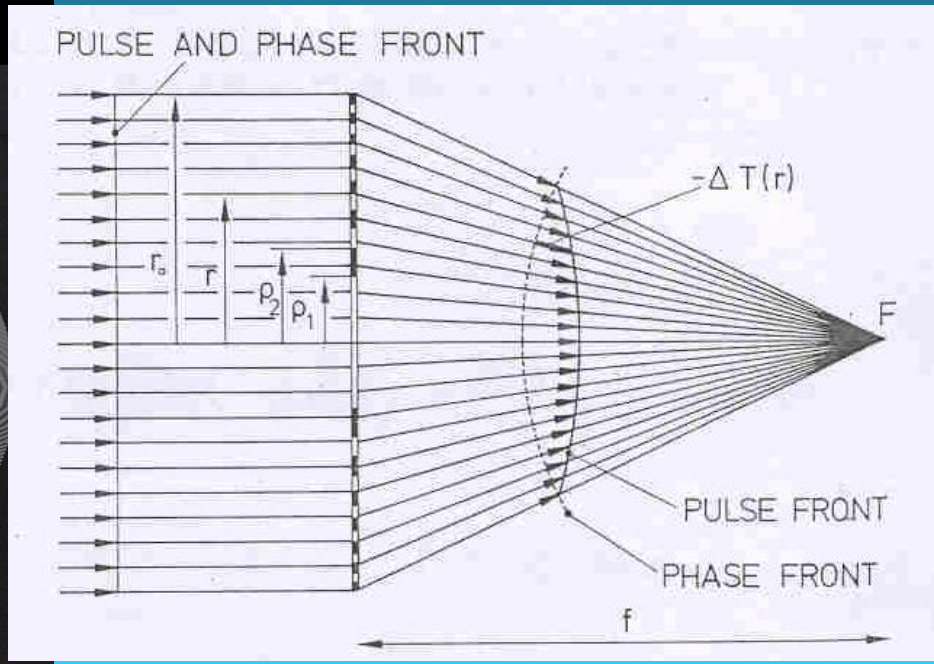

$$\delta_m = [\, \delta_{i,m}^{\,2} + \delta_r^{\,2} + \delta_c^{\,2} \,]^{1/2} = [\, (1.22 \cdot dr_n / m)^2 + (s \cdot f/L)^2 + (D \cdot \Delta E/E)^2 \,]^{1/2}$$

Available for Super B: dr_n=>below 10 nm, s=> 30 um, f/L=1/500-1/1000 , $\Delta E/E = 10^{-4}$

Example: High efficient ZP

(E. Di Fabrizio et al Nature 2009)

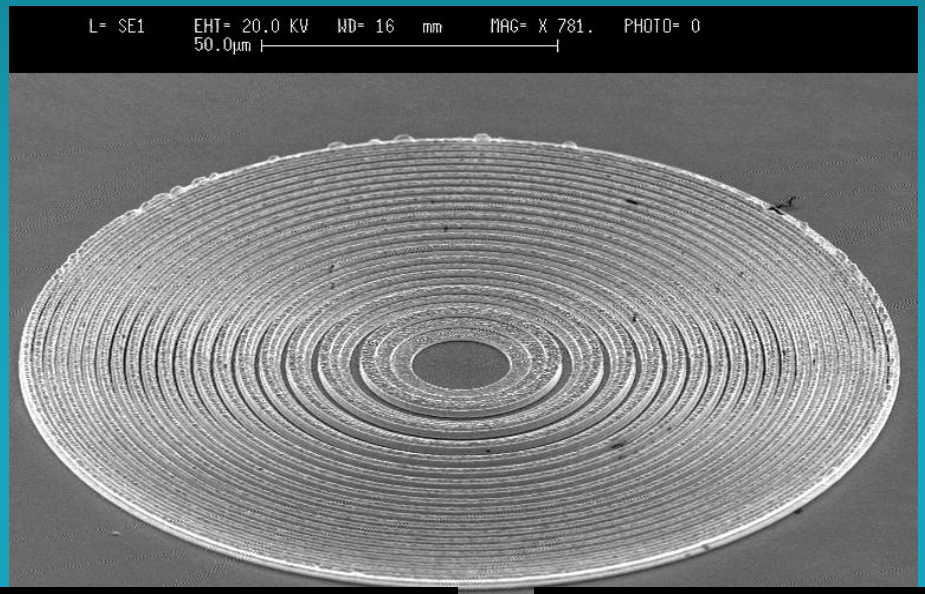

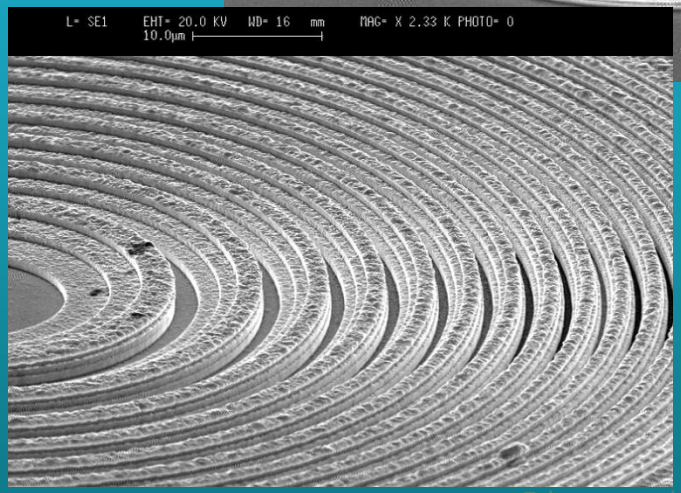

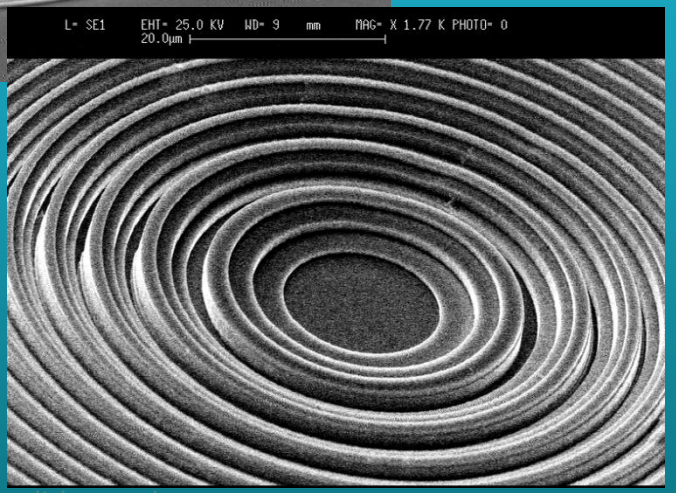

Nanoscale X-ray imaging

David Attwood et al.

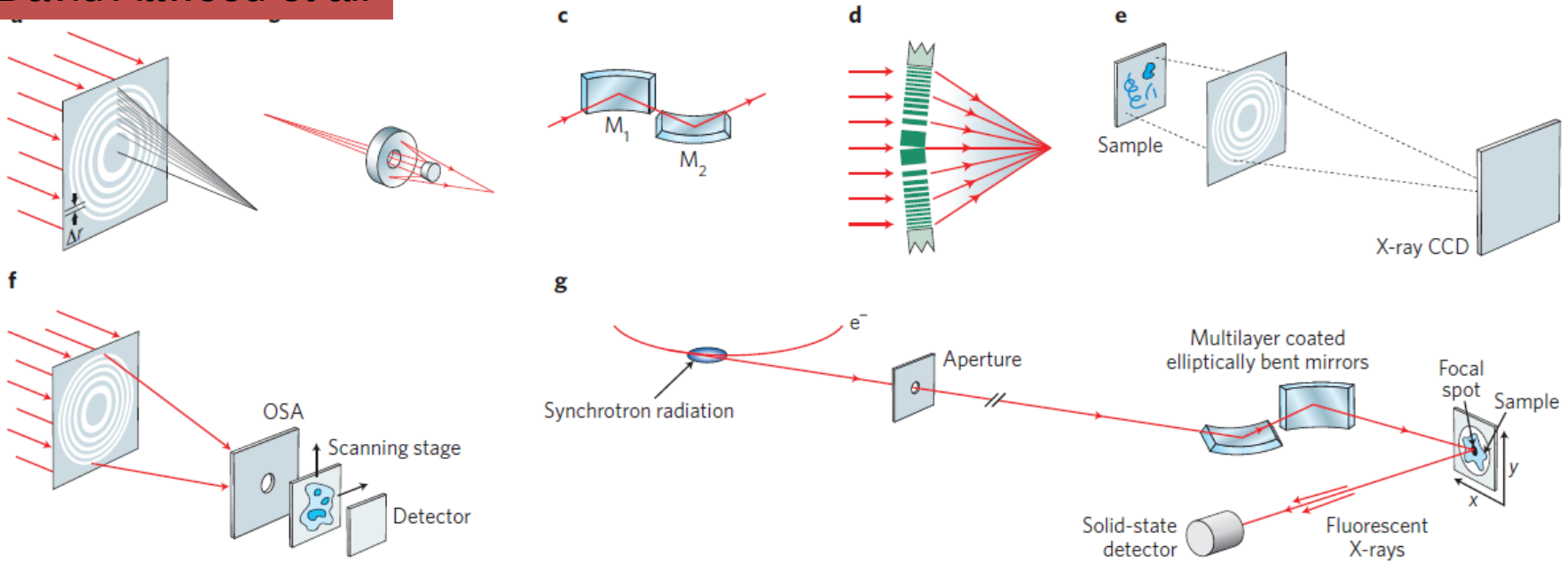

Figure 1 | Four common X-ray microscopy optics (a–d) and three common image-forming systems (e–g). a, A Fresnel zone plate lens is a circular diffractive structure that can be used for focusing or imaging X-rays, shown here as a focusing element. With spatially coherent illumination, the focal spot size is set by the outer zone width Δr, with a Rayleigh resolution of $1.2\Delta r$. **b**, A multilayer-coated two-bounce Schwarzschild reflective objective for focusing or imaging. The multilayer coating generally limits the efficiency to wavelengths greater than several nanometres. **c**, A KB glancing incidence mirror pair (M_1, M_2) for focusing hard X-rays. Multilayer coatings are sometimes used for photon energy selection and to increase the angles of operation. **d**, A multilayer Laue lens for focusing X-rays. This optic uses multilayer coatings to achieve thin, very high aspect ratio zones, of variable period, which are suitable for the nanoscale focusing of hard X-rays. **e**, Full-field TXM showing a back-illuminated sample, with transmitted photons imaged at high magnification to an X-ray-sensitive CCD array detector by a high-resolution zone plate. Limits on the angular illumination cone are used to control zero and higher order radiation. Illumination control is important for achieving maximum resolution. **f**, Zone-plate-based STXM showing X-rays focused to a small spot on a raster-scanned sample, with a detector recording transmitted photons as a function of scanning time. An order-sorting aperture (OSA) is used in conjunction with a thick central zone to block zero and higher order radiation[1]. **g**, Scanning μ-XRF microprobe based on a multilayer-coated KB mirror pair and bending magnet synchrotron radiation. Alternatively, operating in transmission mode with a high-spectral-resolution crystal monochromator and an upstream undulator as the source, the KB microprobe can be used for a variety of microscale X-ray absorption spectroscopy techniques such as μ-XANES. This system can also be used in transmission mode for μ-XRD. Figure reproduced with permission from: **a–c**,**e–g**, ref. 1, © 2000 Cambridge University Press; **d**, ref. 30, © 2008 AIP.

Biological applications of nanoscale X-ray imaging

David Attwood et al.

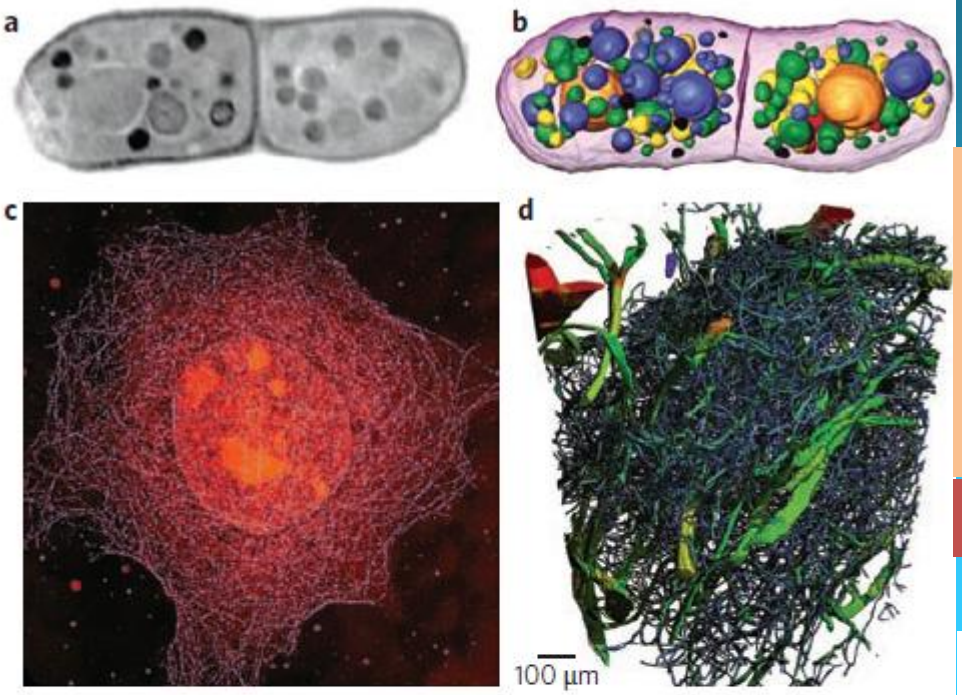

Figure 3 | Biological applications of nanoscale X-ray imaging. a,**b**, A not-yet-separated mother–daughter yeast cell pair, whole and unstained with rapid-freeze cryofixation. Yeast cells are important because they are used as biological model systems for genetic studies. These projection 2D images were taken with a zone plate of 45 nm outer zone width, at 2° intervals covering an angle of 180°, at 517 eV (wavelength of 2.4 nm). Figure **a** shows a soft-X-ray image of an 8.5-µm-wide yeast cell, *Schizosaccharomyces pombe*, extracted as a 2D slice of a reconstructed 3D tomogram obtained at the National Center for X-Ray Tomography full-field microscope at the Advanced Light Source. The image shows a one-voxel-thick slice with grey-scale values corresponding to the observed X-ray absorption coefficient. Figure **b** shows the same cell pair, with sub-cellular components of similar colour correlated according to X-ray attenuation. **c**, The important technique of protein-specific labelling. X-ray absorptive nanoparticles are used to visualize a microtubule network in a whole, hydrated, but chemically fixed EPH4 mouse epithelial cell. The label consists of a silver-enhanced gold nanoparticle of 50 nm diameter, which roughly matches the spatial resolution of the microscope. The image measures 10 µm^2, and was taken at a resolution of 36 nm and a photon energy of 517 eV. Absorption-dependent quantitative colour-coding is used for visualization. The highly absorbing gold/silver labels in blue highlight the linear microtubule network against a less absorptive (and unlabeled) nuclear structure, shown in orange. The relatively high-water-content cytoplasm has low absorption and so appears black. **d**, Hard-X-ray 3D tomographic rendering of the microvascular architecture within the hippocampus region of a mouse brain. Small capillaries are shown in blue, whereas larger blood vessels are shown in red. The reconstructed volume is a cube of 700 µm × 700 µm × 700 µm. A photon energy of 25 keV was use to obtain the data. The spatial resolution is approximately 15 µm. Figure reproduced with permission from: **a**,**b**, ref. 97, © 2008 Elsevier; **c**, ref. 74, © 2001 Wiley. Figure **d** courtesy of M. Stampanoni

Environmental applications of nanoscale X-ray imaging.

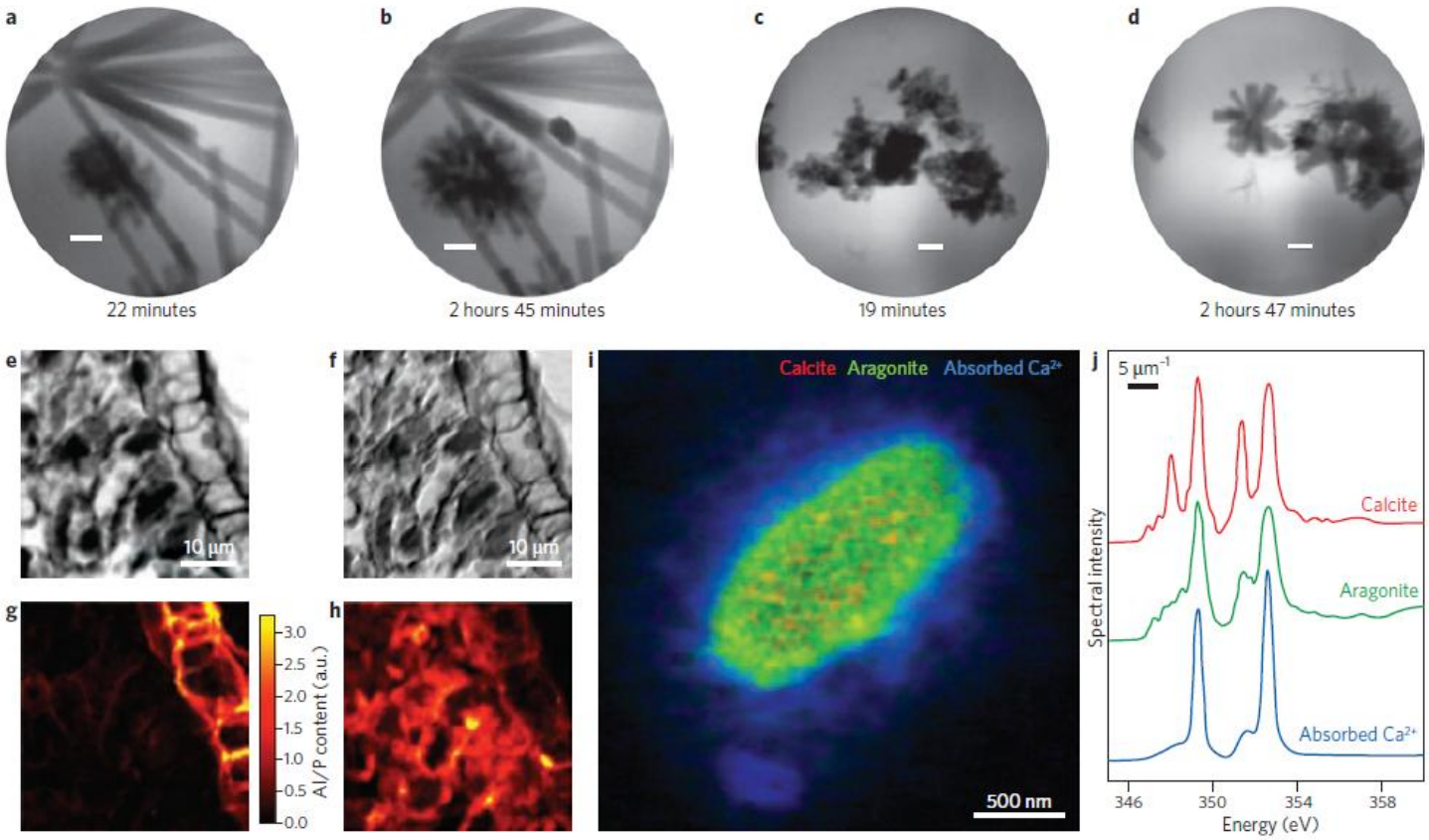

Figure 4 | Environmental applications of nanoscale X-ray imaging. Concrete formation is a major source of air and water pollution. **a**–**d**, Studies of expansive cements containing the admixture C_4A_3S, which is used to alleviate cracking, to determine the morphology as a function of chemistry. In the formula C_4A_3S, C refers to calcium (Ca), A to alumina (Al_2O_3) and S to silica (SiO_2). These soft-X-ray images show the emergence of large ribbon-like structures of hydrating C_4A_3S particles, in fan-like configurations, in saturated solutions of $Ca(OH)_2$ + $CaSO_4{\cdot}H_2O$, as a function of hydration time. Images are in the absence (**a**,**b**) and presence (**c**,**d**) of 10% $Ca(OH)_2$. The images show how ribbon size is strongly affected by chemistry. The images were obtained at 520 eV (wavelength of 2.4 nm) using the full-field soft-X-ray microscope at the Advanced Light Source. The scale bars are 1 µm wide. **e**–**h**, The study of aluminium toxicity in tea leaves (*Camellia sinensis*) using X-ray images and elemental maps at 1.7–2.2 keV. Slices of tea leaves reveal that the aluminium concentration is high in the epidermal (Epi) cell walls but low in the mesophyll (Mes) cell walls. The much lower content of phosphorous in the epidermal cells compared with the mesophyll cells indicates that phosphorous plays a negligible role in the sequestration of aluminium. Figure **e**,**f** shows brightfield (BF) and differential phase contrast (DPC) X-ray images of slices from tea leaves, respectively. Figure **g**,**h** shows aluminium and phosphorus low-energy X-ray fluorescence maps, respectively. **i**,**j**, From studies of pollution and potential carbon sequestration in the hydrosphere, STXM soft-X-ray spectromicroscopy is used to map concentrations of calcite, aragonite and calcium ions in the extracellular polysaccharide matrix of freshwater cyanobacteria *Synechococcus leopoliensis*. Calcite is shown in red, aragonite in green, and adsorbed calcium ions in blue. Curves are arbitrarily separated vertically for visual clarity. Figure reproduced with permission from: **a**–**d**, ref. 79, © 2009 Elsevier; **e**–**h**, ref. 81, © 2010 Springer; **i**,**j**, ref. 82, © 2009 Elsevier.

Full-field imaging microscope operating in DIC mode – Optical setup

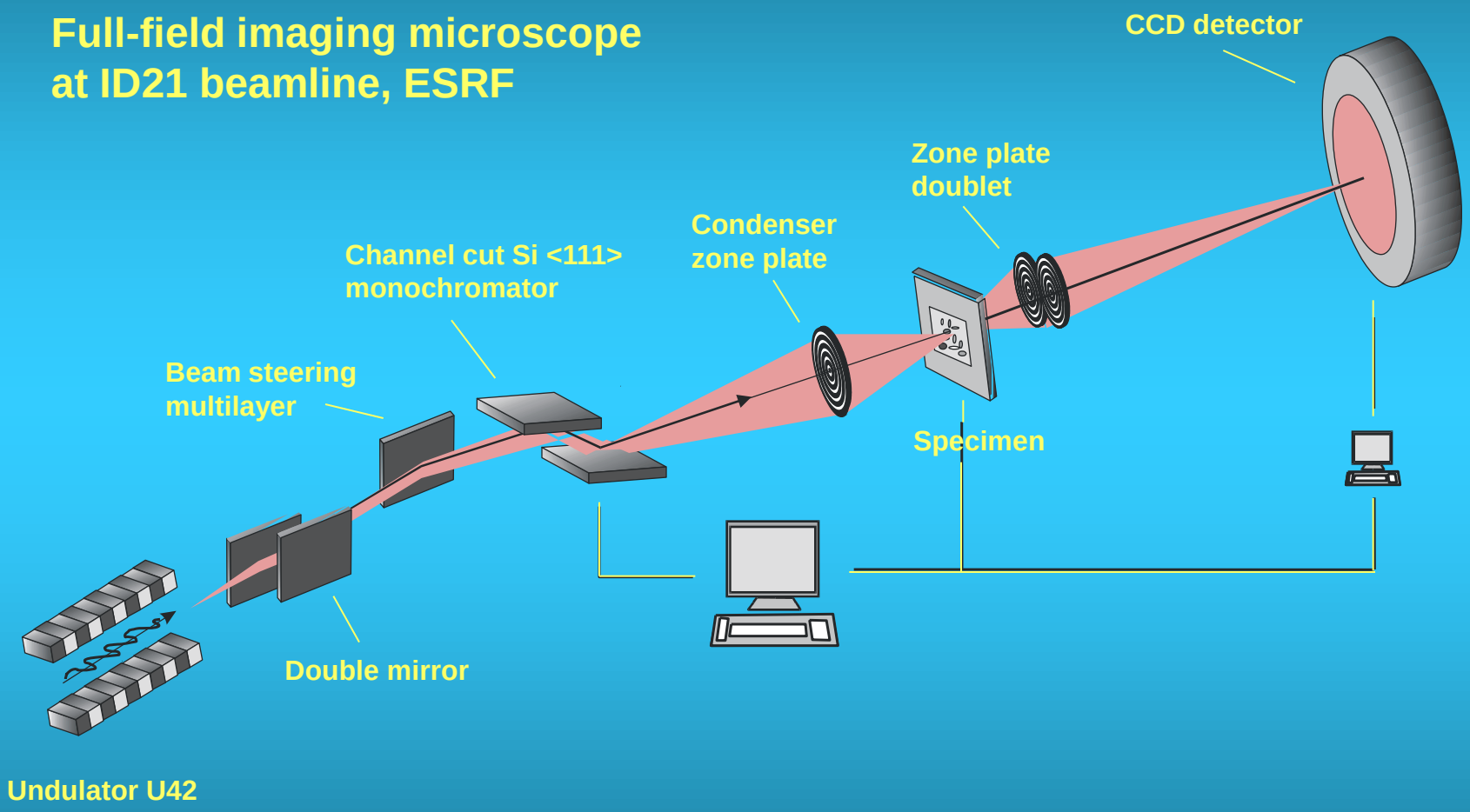

DIC with the scanning X-ray microscope: Optical setup

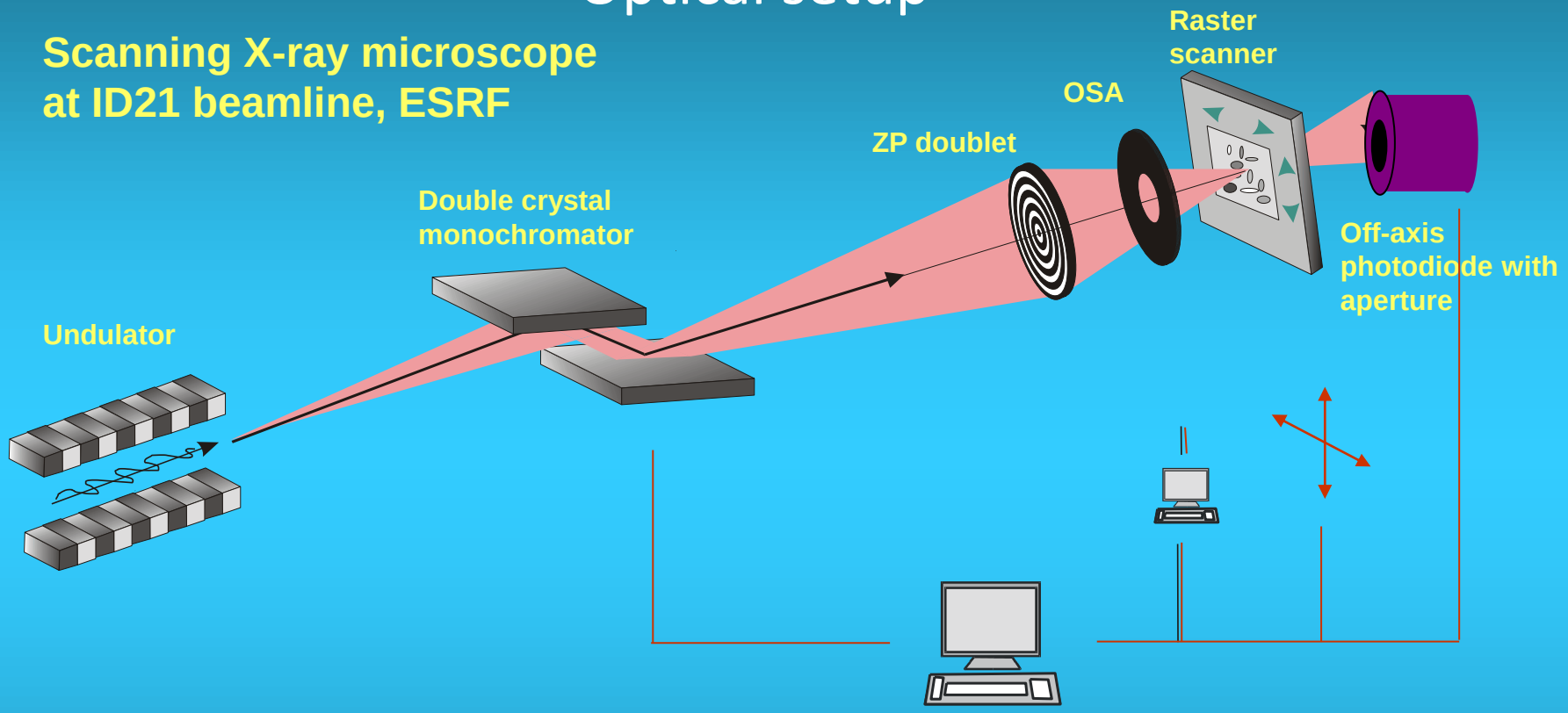

General scheme in wavefront engineering

DOEs are optical elements that convert the input wave into an output wave, reflected or transmitted, with a desired distribution of its amplitude, phase or polarization, by DIFFRACTION.

Using computer design techniques, the wave fields are represented as computer data to design diffractive coded optics that carry out complex optical functions that cannot be obtained otherwise.

E. Di Fabrizio et al. MRT 2005

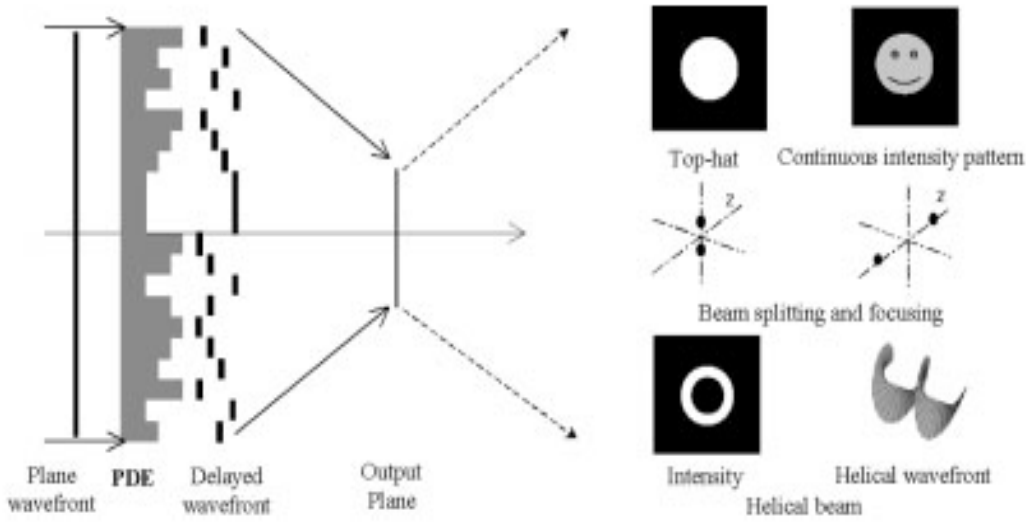

Fig. 1. Phase modulation principle and examples of optical functions accomplished by PDEs.

Complete X-ray- beam shaping

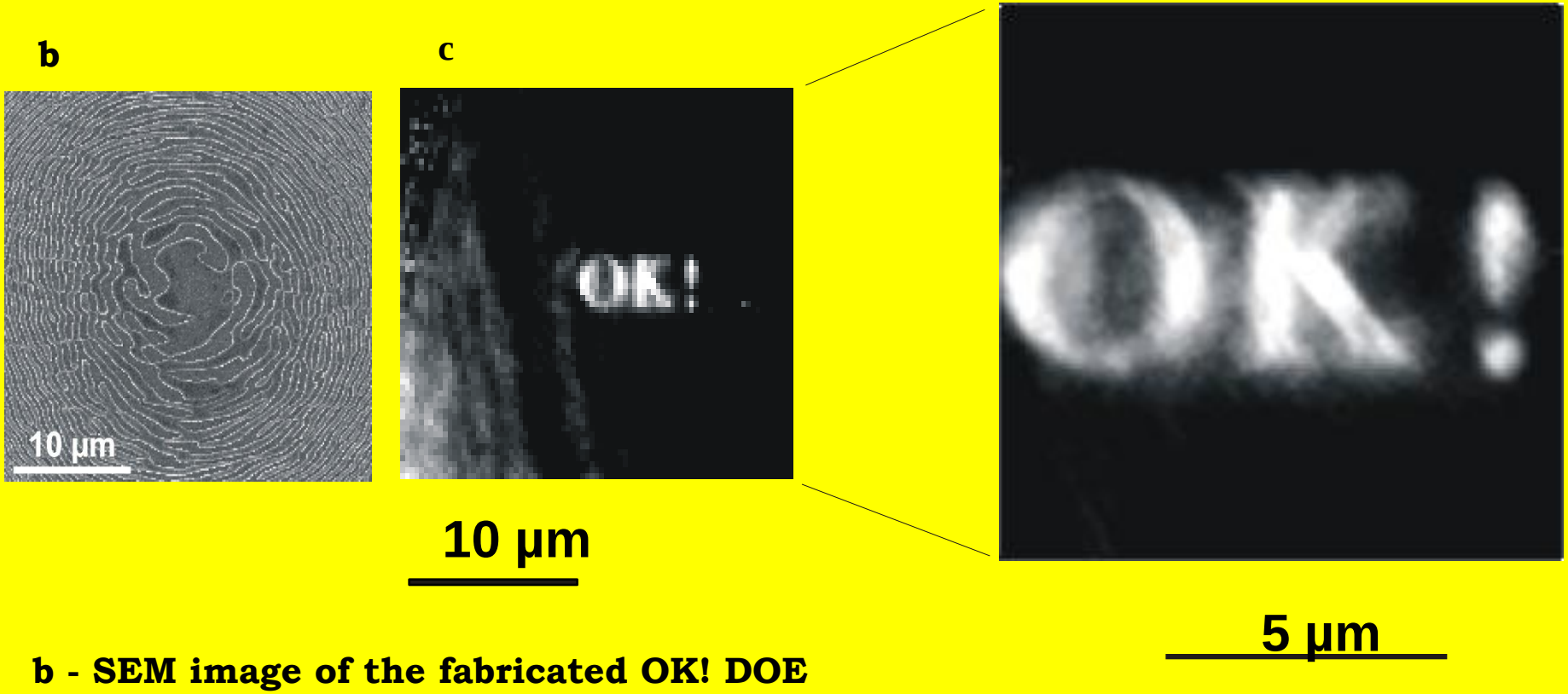

b - SEM image of the fabricated OK! DOE
c - The intermediate image formed by the DOE at the focal plane located at 50 mm is magnified 150 times on a CCD detector by a ZP that acts as an objective lens

E. Di Fabrizio, D. Cojoc, S. Cabrini, B. Kaulich, J. Susini, P. Facci, T. Wilhein, Opt. Express 11 (2003) 2278.

DOE beamshaping for X-ray

Optical scheme and calculated layout

of 3 DOE's that generate 2 and 4 spots

(a-b) on the same focal plane, and 2

spots along the same optical axis(c)

(d)Full beamshaping

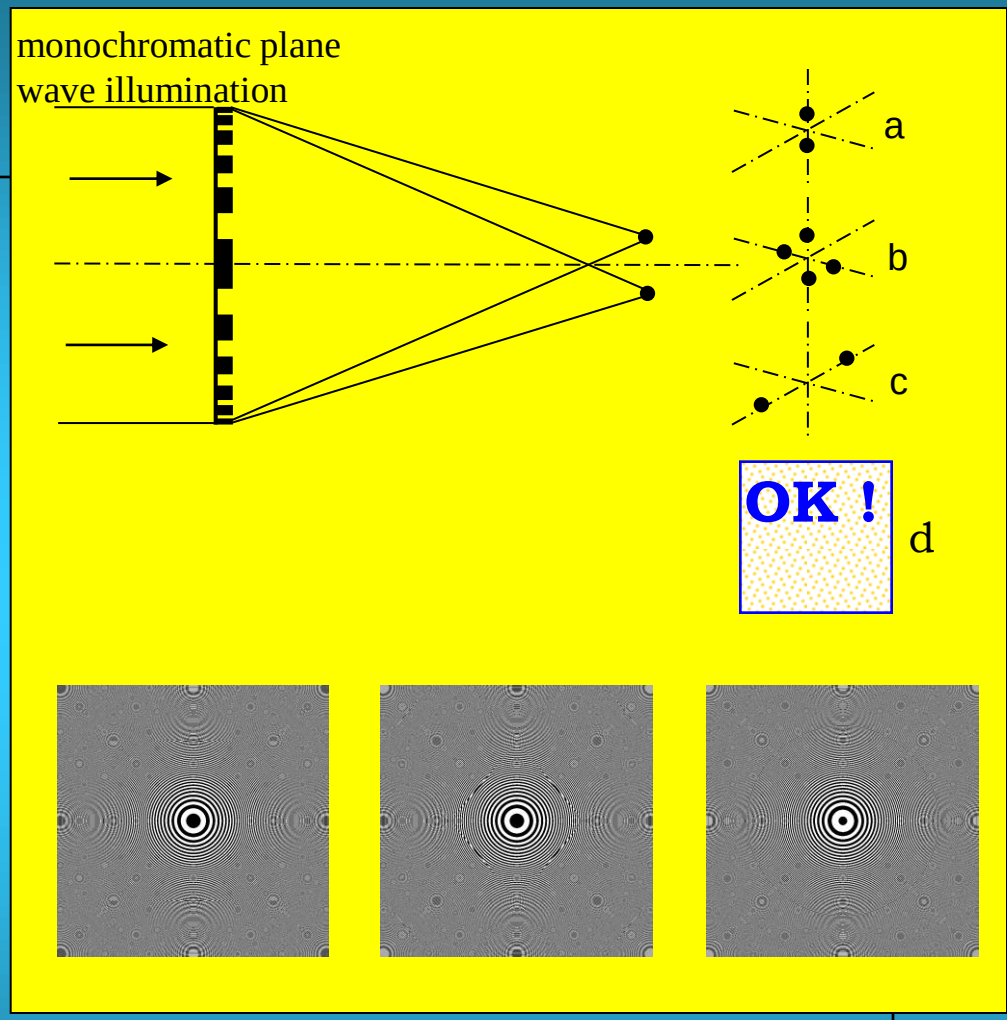

The calculations are referred to a photon energy of 4 KeV and 5 cm focal length

Development of multi-spot X-ray DOE

Calculated pattern of a 4 spot ZP

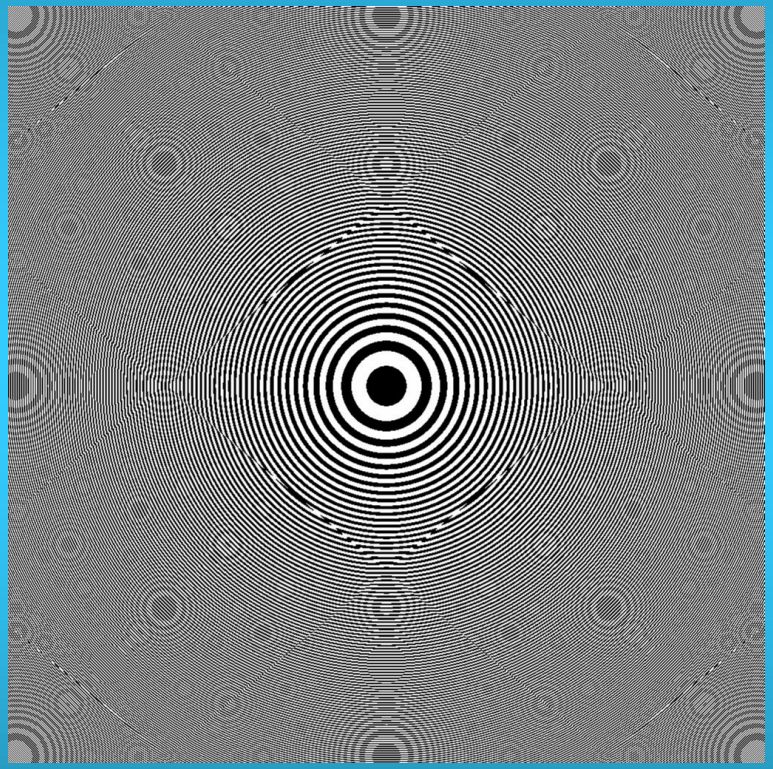

DIC visible light micrograph of 4-spot ZP

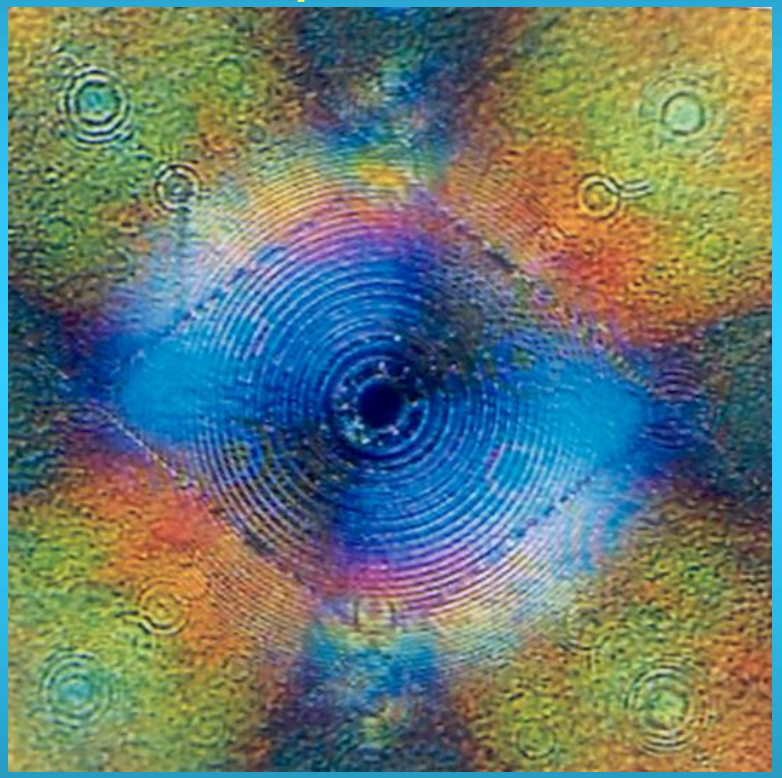

DOE size 0.1 x 0.1 mm2, pixel size: 100 nm, energy 4 keV

designed and generated by the Lilit beamline group (2001)

Development of multi-spot X-Ray DOE

SEM pictures showing an overview of the DOE (DOE area is 100x 100 μm²) and details of the outermost area whose resolution is below 100 nm

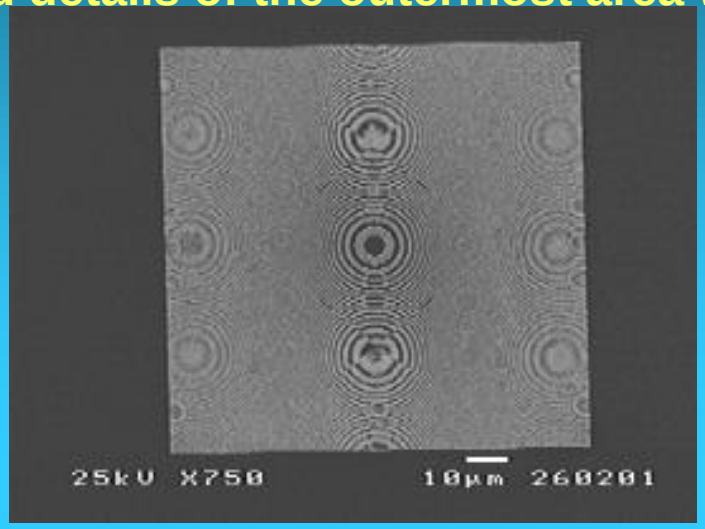

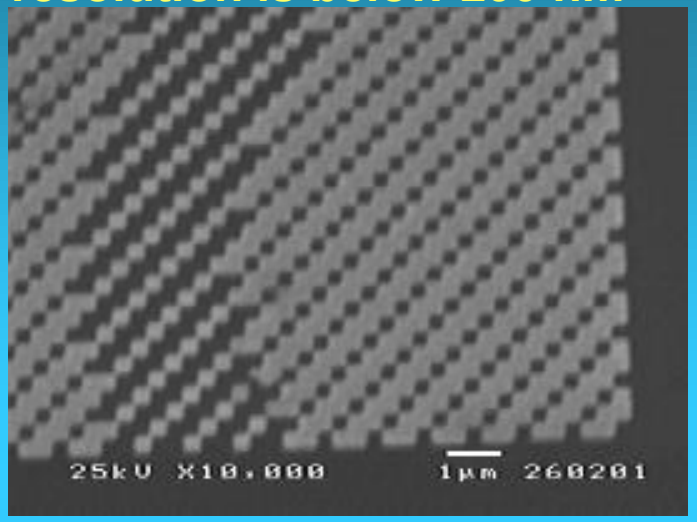

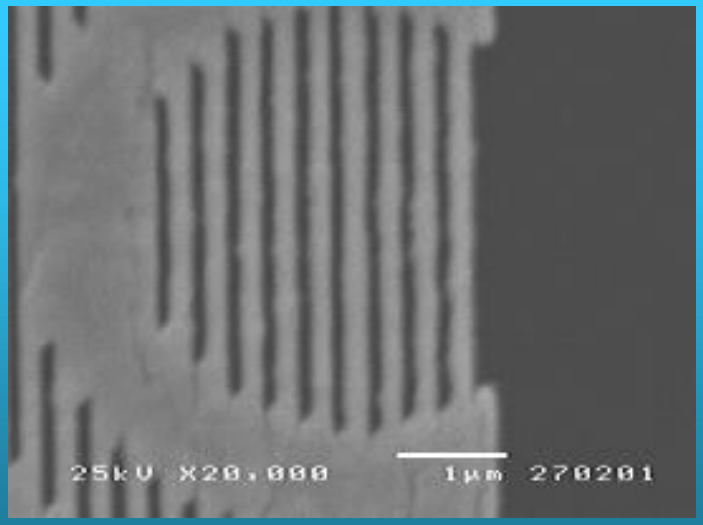

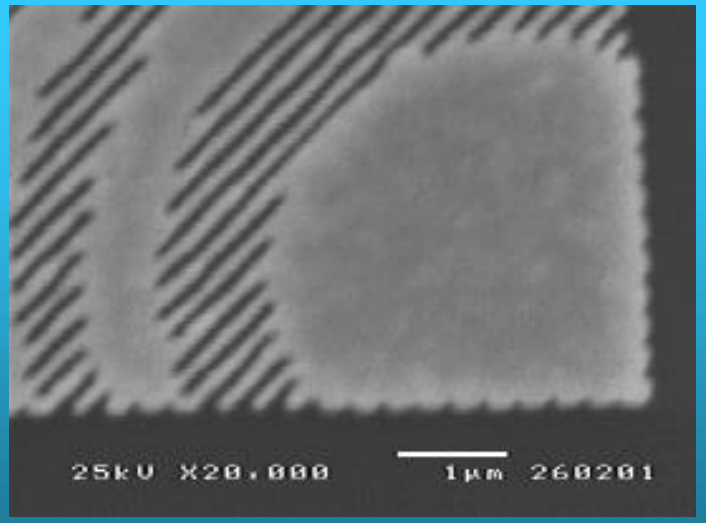

Contrast in X-ray microscopy

Refractive index in X-ray region: $n = 1 - \delta + i\cdot\beta$

$\delta \rightarrow$ phase shift $\beta \rightarrow$ absorption

example: polyimide

photon energy [eV]	δ	β	δ / β
100	$2.3 \cdot 10^{-2}$	$4.9 \cdot 10^{-3}$	4.7
500	$1.1 \cdot 10^{-3}$	$3.2 \cdot 10^{-4}$	3.4
5000	$1.2 \cdot 10^{-5}$	$7.1 \cdot 10^{-8}$	170

$\rightarrow$ phase sensitive techniques superior to absorption contrast !

Motivation for microscopy techniques using phase information

Absorption contrast: $\sim E^{-3}$

Phase contrast: $\sim E^{-1}$

Use of phase shifting, real part of refractive index

- **orders of magnitude higher contrast**
- **tremendous reduction of dose applied to object**
- **additional transmission information on low side of absorption edges (XANES, XRF !)**

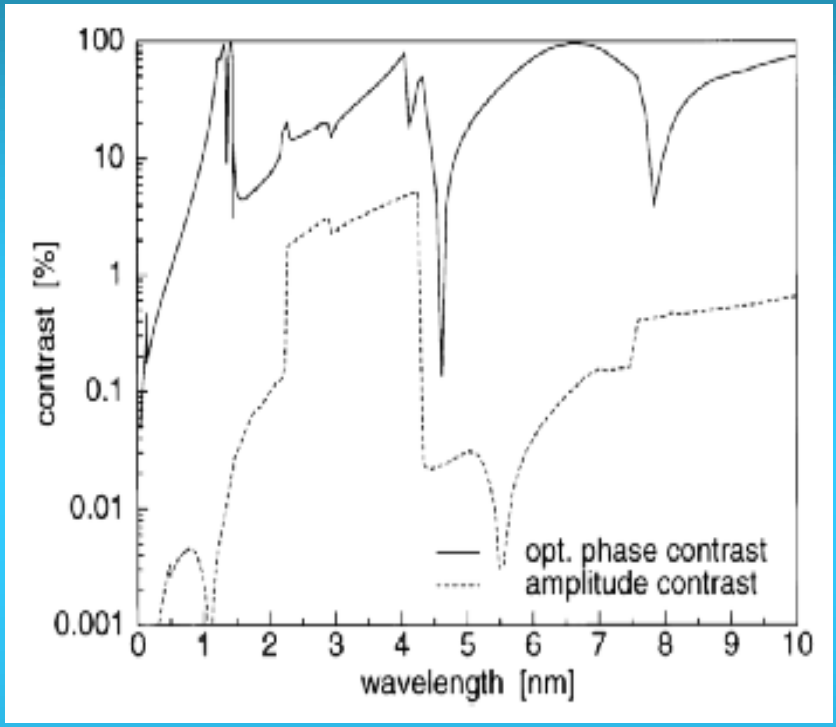

Amplitude and phase contrast for a model protein $C_{94}H_{139}N_{24}O_{31}$

Field Intensity in the DIC image

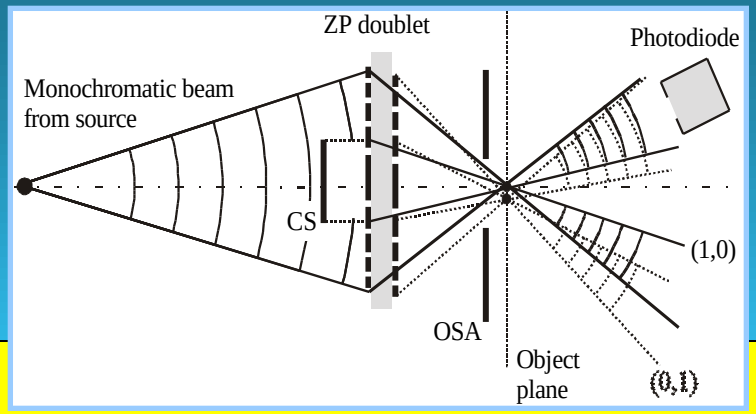

$$i(x,y) = a_1 \sin^2 \left[0.5 \left\{\phi(x - \Delta x, y) - \phi(x + \Delta x, y)\right\} + \Delta\theta\right]$$

If the shear Δx **very small (differential) compared to the size of the details of the specimen (or the resolution of the ZP) ==> the phase difference can be written as a phase gradient:**

$$i(x,y) = a_1 \sin^2 \left(\Delta x \, \frac{\partial \phi(x,y)}{\partial x} + \Delta\theta \right)$$

With DOE is possible to control the contrast through the bias $\Delta\Theta$

Optical setup of DIC full field microscope

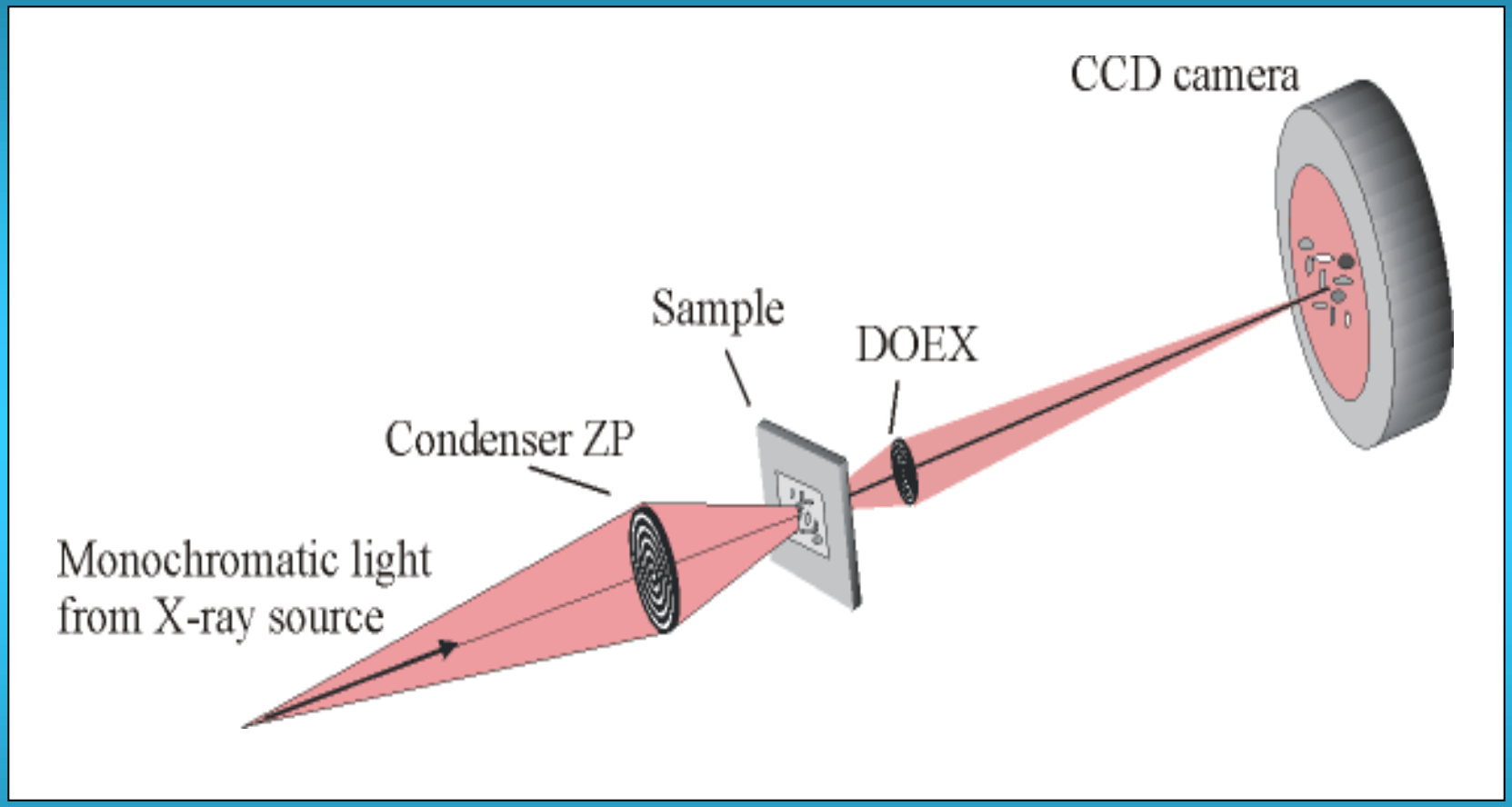

Scanning X-ray microscope at ID21 beamline, ESRF

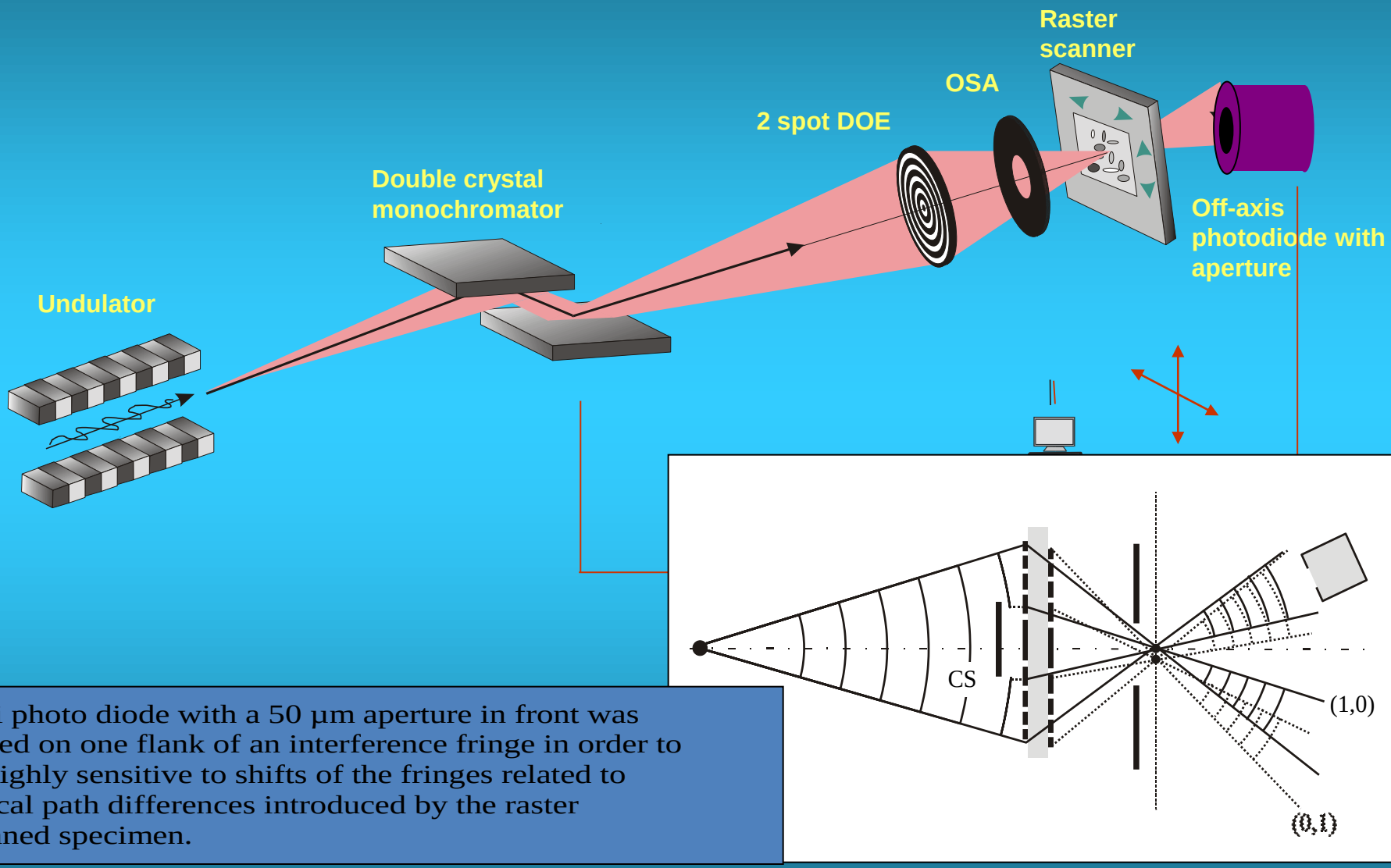

A Si photo diode with a 50 µm aperture in front was placed on one flank of an interference fringe in order to be highly sensitive to shifts of the fringes related to optical path differences introduced by the raster scanned specimen.

PMMA test structures

test structures(a=squares, b=toroids) 1 μm thick with a transmission of 99.99 % @ 4 keV

a

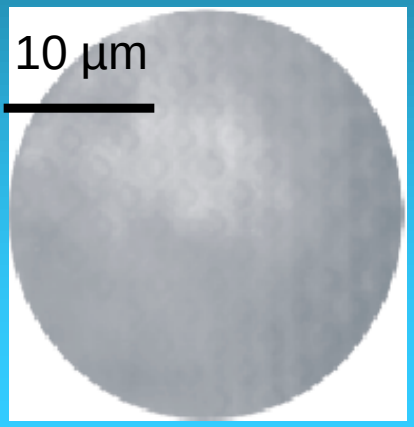

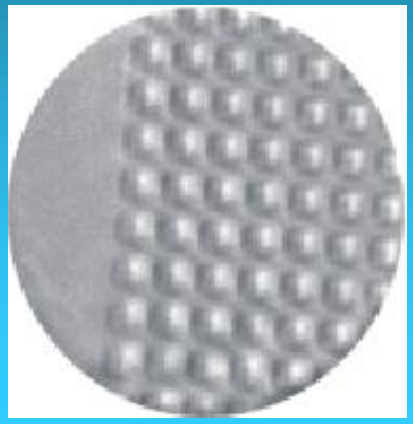

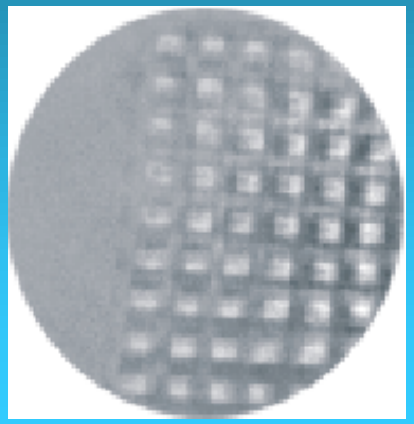

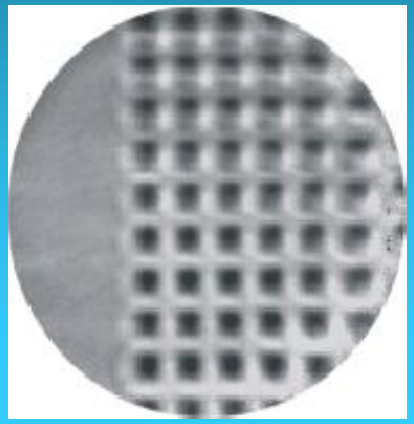

Objective lens :

ZP

2 confocal spots DOE

4 confocal spots DOE

2 coaxial spots DOE

b

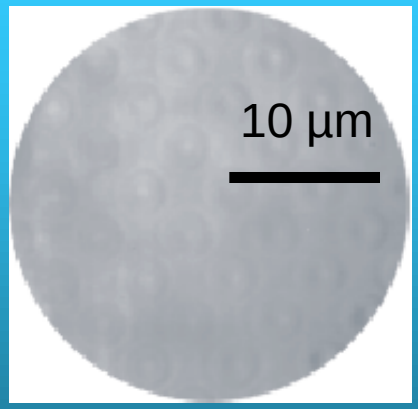

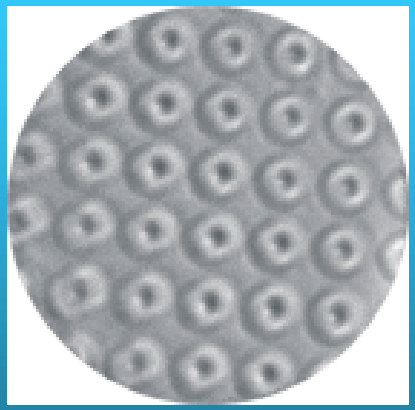

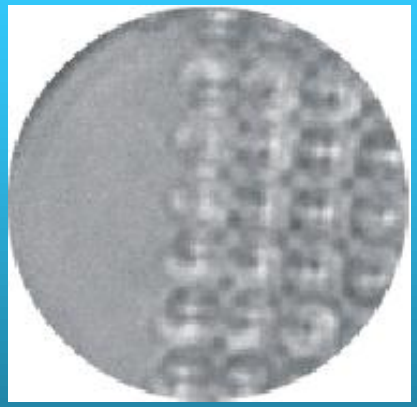

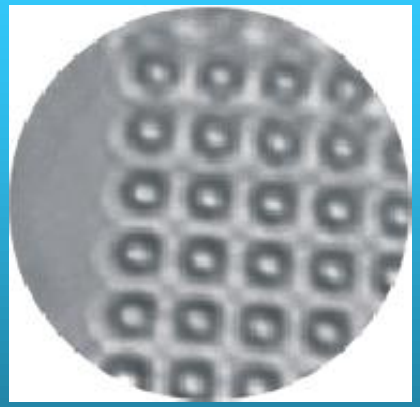

2 spot DIC&XRF measurements

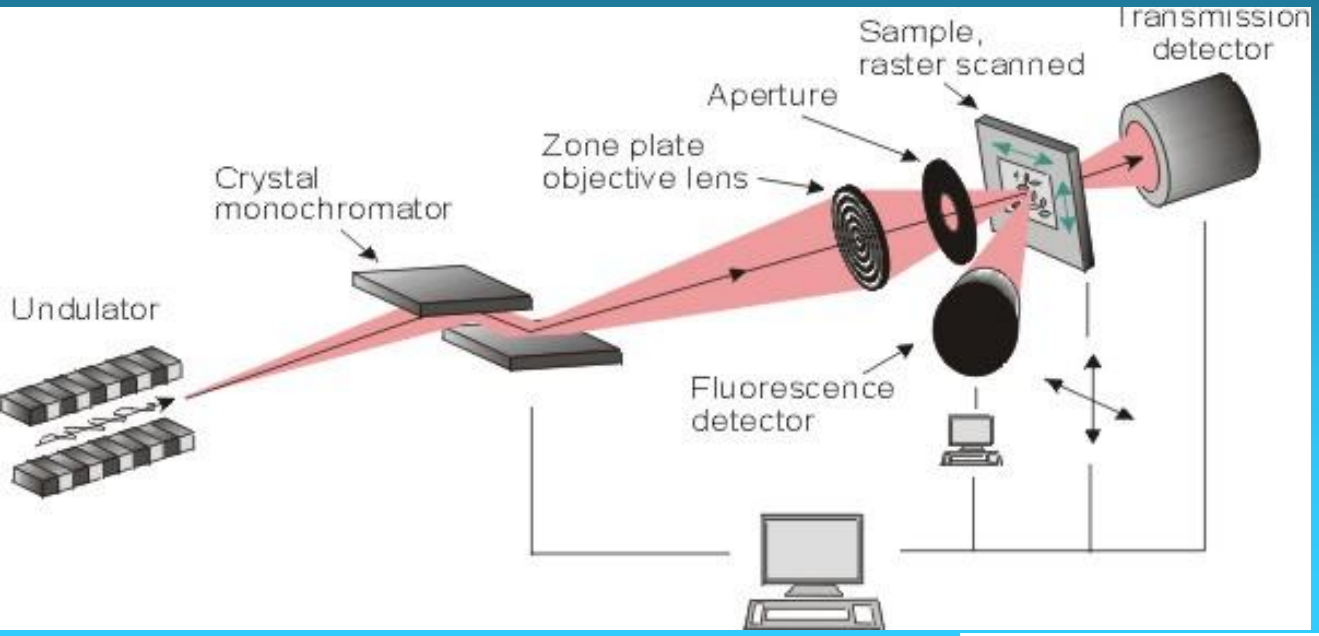

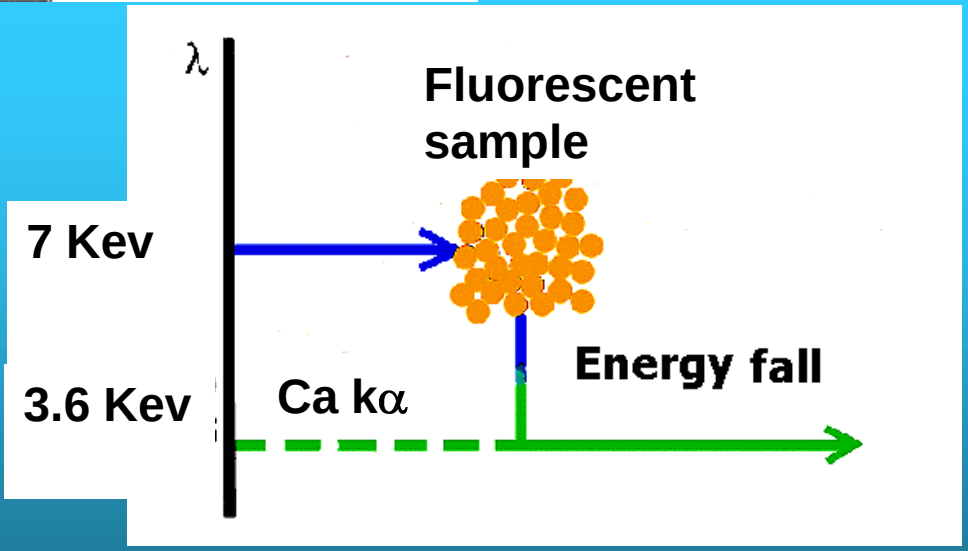

Air Pollution SiO2 fiber Filter(Trieste)
2 spot DIC&XRF measurements

7.2 KeV X-ray

Absorption contrast

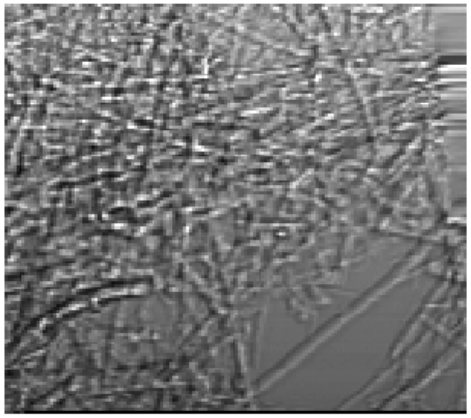

Diff. Interf. contrast

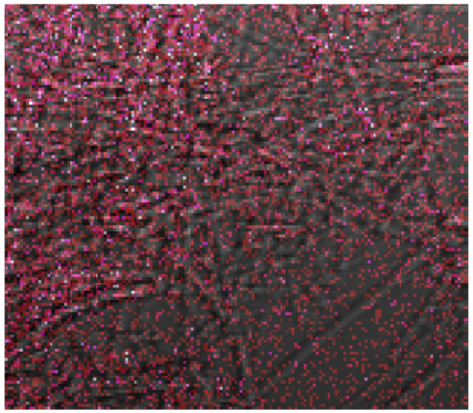

Cr XRF map

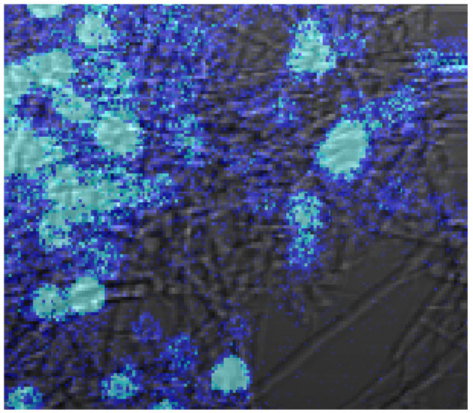

Fe XRF map

Id21, ESRF, Mi578, 7.2 keV, 160 x 145 (?) px, 100 x 100 µm
thin sample

4 KeV X-ray

Absorption contrast

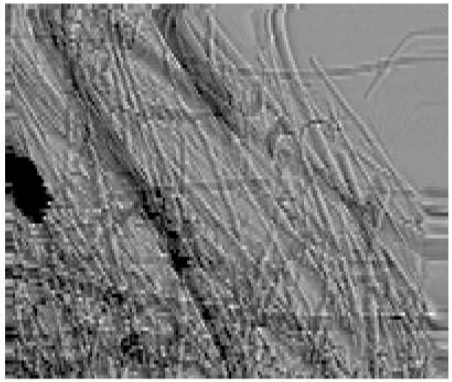

Differential interference contrast

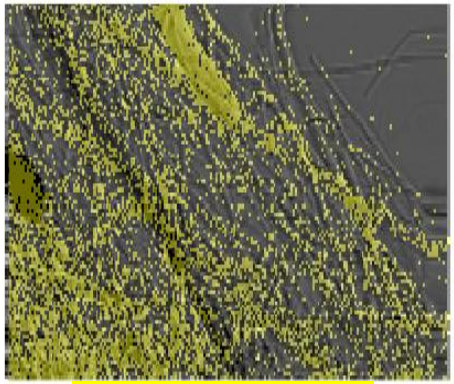

Ca XRF map

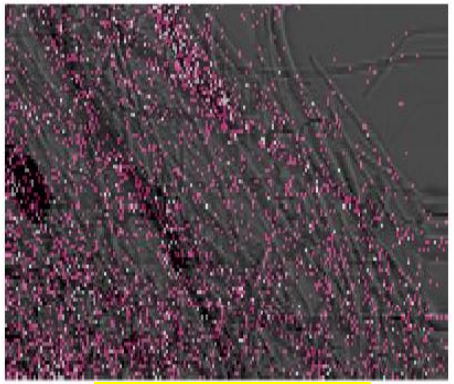

K XRF map

Field Intensity in the DIC image

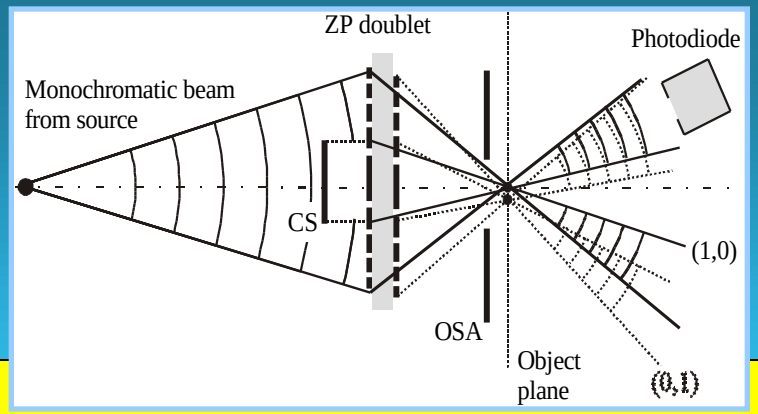

$$i(x,y) = a_1 \sin^2 \left[0.5 \left\{\phi(x - \Delta x, y) - \phi(x + \Delta x, y)\right\} + \Delta\theta\right]$$

If the shear Δx **very small (differential) compared to the size of the details of the specimen (or the resolution of the ZP) ==> the phase difference can be written as a phase gradient:**

$$i(x,y) = a_1 \sin^2 \left(\Delta x \, \frac{\partial \phi(x,y)}{\partial x} + \Delta\theta \right)$$

With DOE is possible to control the contrast through the bias $\Delta\Theta$

Bias retardation in DIC

$$i(x,y) = a\sin^2\left(\Delta x\frac{\partial\phi(x,y)}{\partial x} + \Delta\theta\right)$$

Phase (radians)

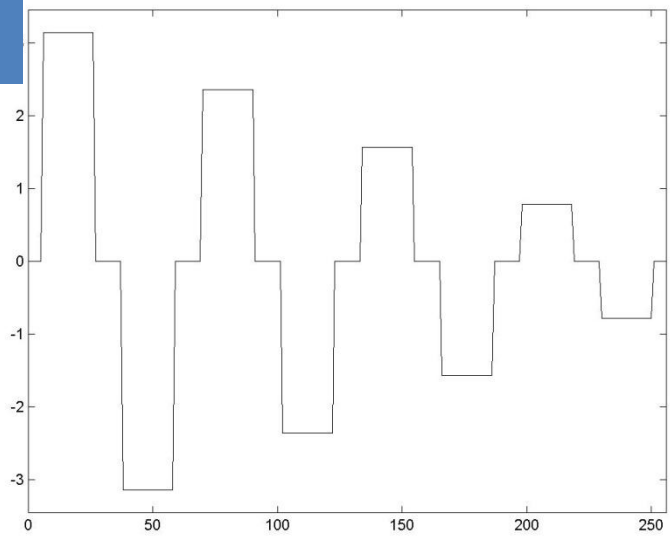

Intensity (a.u.)

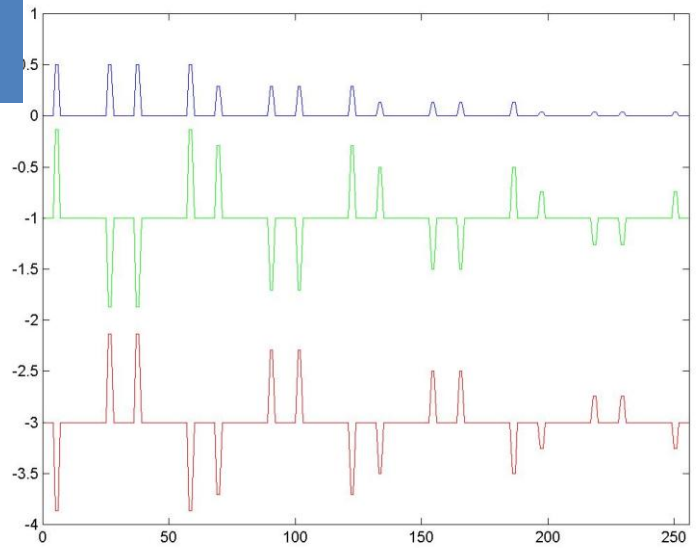

(a) The phase function of a one dimensional object described in 250 pixels;
(b) Intensity distributions obtained with the same shear $\Delta x = 2$ but different bias values: $\Delta\theta = 0$ - first line, $\Delta\theta = \pi/4$ - second line, and $\Delta\theta = 3\pi/4$ - third line;
the signals are offset by 2 a.u. for a clear representation

DOEs producing the same beam shearing (1 mm) but different bias: a) no bias, b) bias = π at 1 m from the DOE (DOE size= 2 cm, described in 480 pixels)

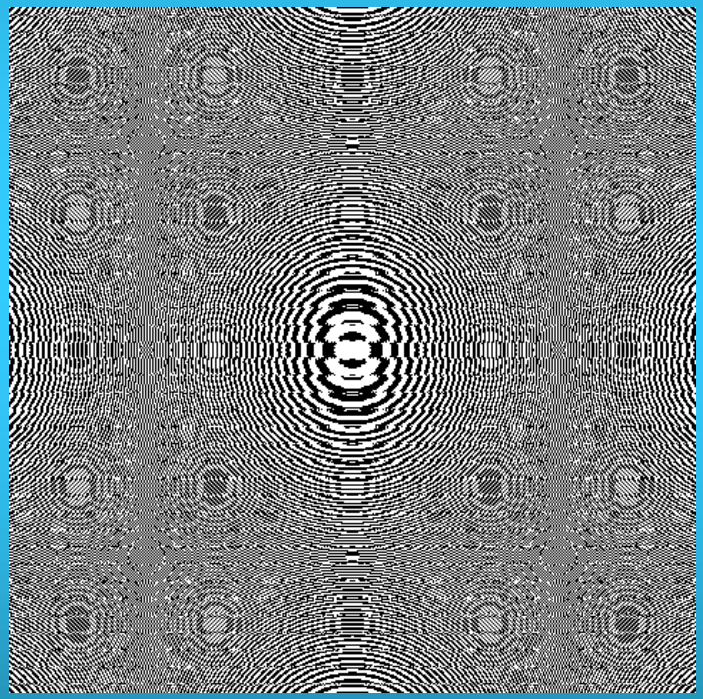

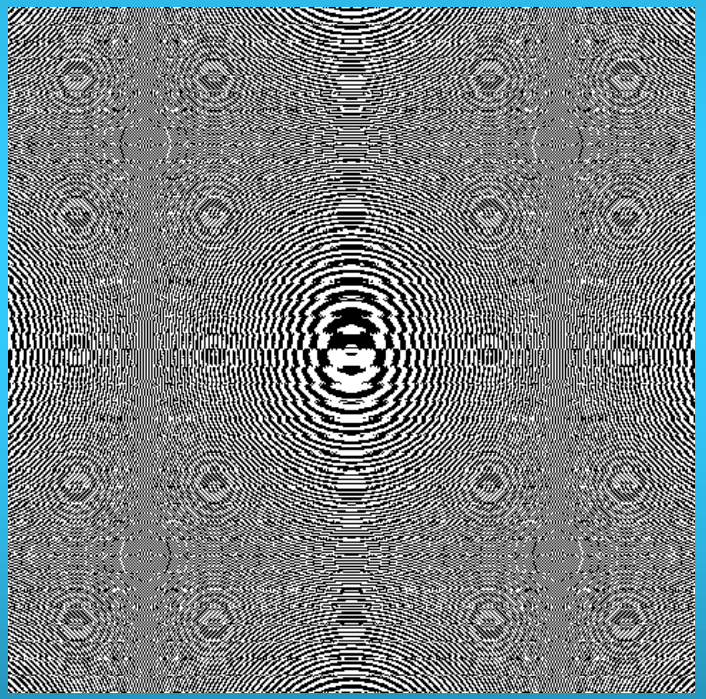

Spherical wave propagation approach

To calculate the phase function Φ_{PDE}, we assume that the light source which illuminates the PDE and the intensity distribution produced by the PDE can be described by point sources generating spherical waves

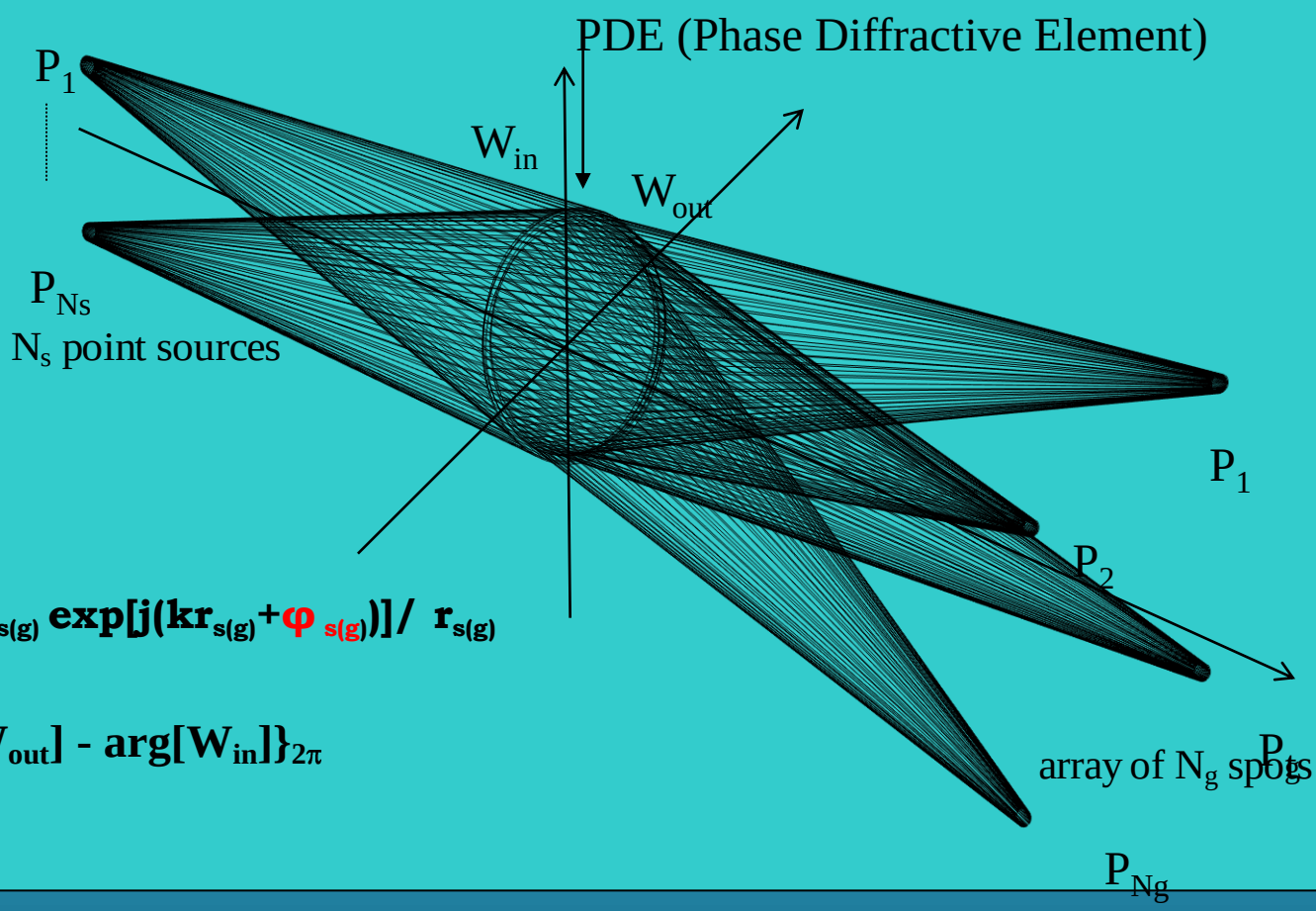

$$W_{in(out)} = \sum_{s(g)} a_{s(g)} \exp[j(kr_{s(g)} + \varphi_{s(g)})] / r_{s(g)}$$

$$\Phi_{PDE} = \{\arg[W_{out}] - \arg[W_{in}]\}_{2\pi}$$

KLA 8100
HVTEST/LINES/HVTEST
Date: 7/30/03 Time: 12:02 PM

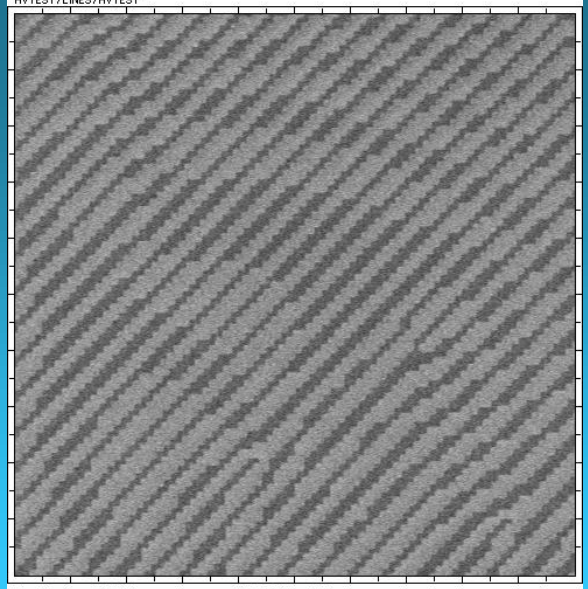

Magnification: 9.38 kX
Field Of View: 16.0 μm

KLA 8100
HVTEST/LINES/HVTEST
Date: 7/30/03 Time: 12:15 PM

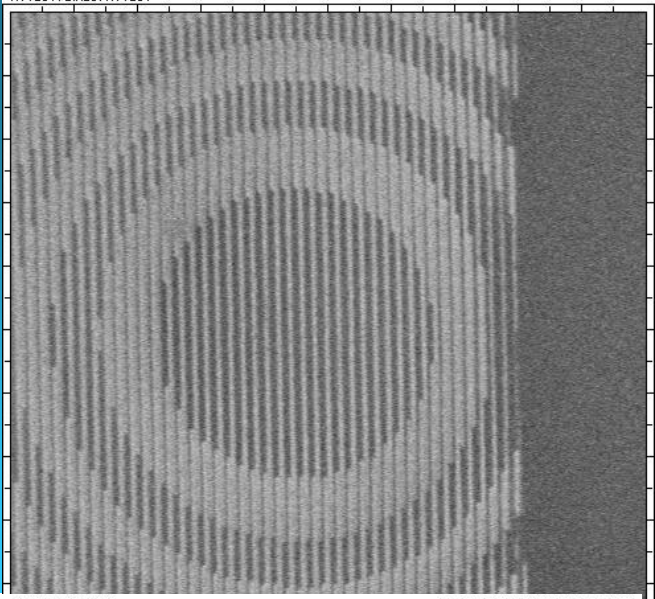

KLA 8100
HVTEST/LINES/HVTEST
Date: 7/30/03 Time: 11:53 AM

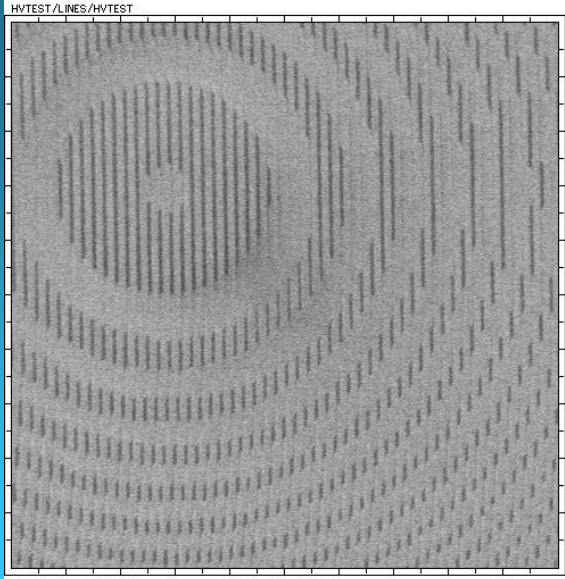

Magnification: 12.50 kX
Landing Voltage: 405.3 V
EF Settings: -203.4 V
Lot: C030543-CHK
Beam File: 400-SE-20
Comment:
Field Of View: 12.0 μm
Wafer X: -13518.9 μm
Wafer Y: -10012.4 μm
Row: 1
Column: 0
Micron Bar: 2 μm
Die X: 23981.1 μm
Die Y: 12487.6 μm
Sub Row: 0
Sub Column: 0

KLA 8100
HVTEST/LINES/HVTEST
Date: 7/30/03 Time: 12:13 PM

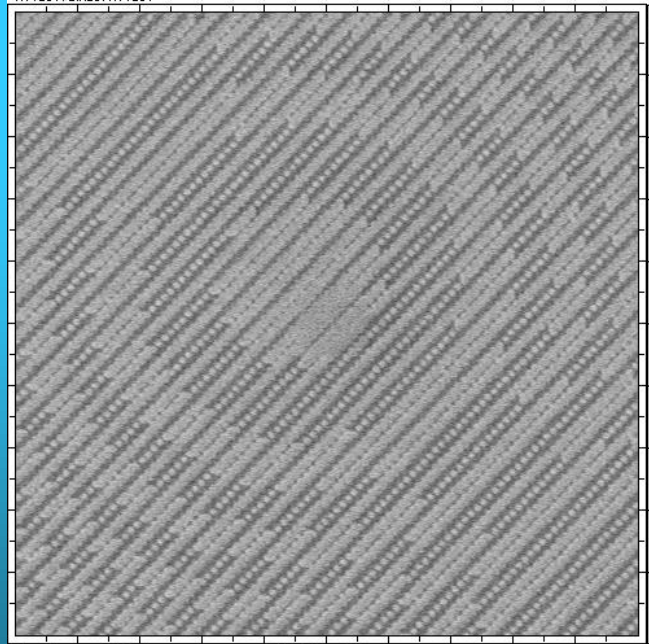

Magnification: 9.38 kX
Landing Voltage: 405.3 V
EF Settings: -203.4 V
Lot: C030543-CHK
Beam File: 400-SE-20
Comment:
Field Of View: 16.0 μm
Wafer X: 6606.1 μm
Wafer Y: -11929.6 μm
Row: 1
Column: 1
Micron Bar: 3 μm
Die X: 19106.1 μm
Die Y: 10570.4 μm
Sub Row: 0
Sub Column: 0

KLA 8100
HVTEST/LINES/HVTEST
Date: 7/30/03 Time: 11:52 AM

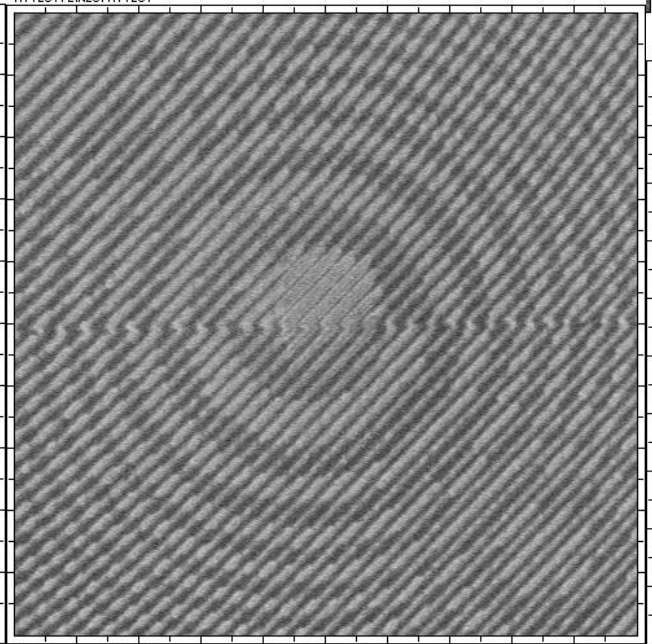

Magnification: 12.50 kX
Landing Voltage: 405.3 V
EF Settings: -203.4 V
Lot: C030543-CHK
Beam File: 400-SE-20
Comment:
Field Of View: 12.0 μm
Wafer X: -13510.4 μm
Wafer Y: -13048.7 μm
Row: 1
Column: 0
Micron Bar: 2 μm
Die X: 23989.6 μm
Die Y: 9451.3 μm
Sub Row: 0
Sub Column: 0

KLA 8100
HVTEST/LINES/HVTEST
Date: 7/30/03 Time: 12:03 PM

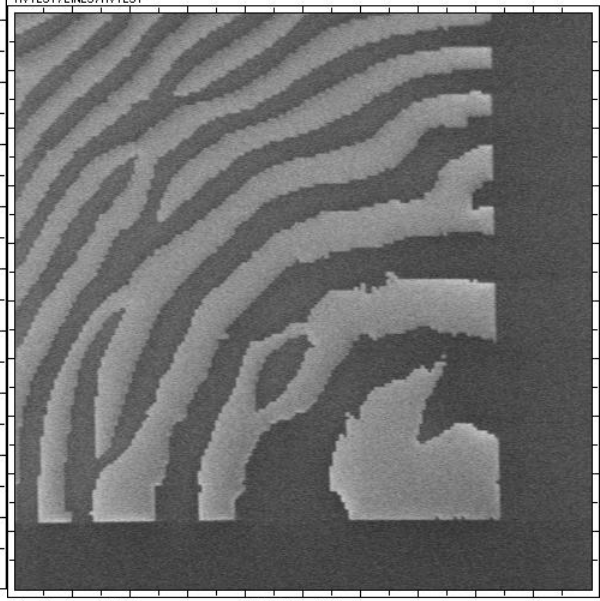

Magnification: 4.69 kX
Landing Voltage: 405.3 V
EF Settings: -203.4 V
Lot: C030543-CHK
Beam File: 400-SE-20
Comment:
Field Of View: 32.0 μm
Wafer X: -3380.1 μm
Wafer Y: -11076.1 μm
Row: 1
Column: 1
Micron Bar: 5 μm
Die X: 9119.9 μm
Die Y: 11423.9 μm
Sub Row: 0
Sub Column: 0

50 nm smaller pixel size with 30 nm details

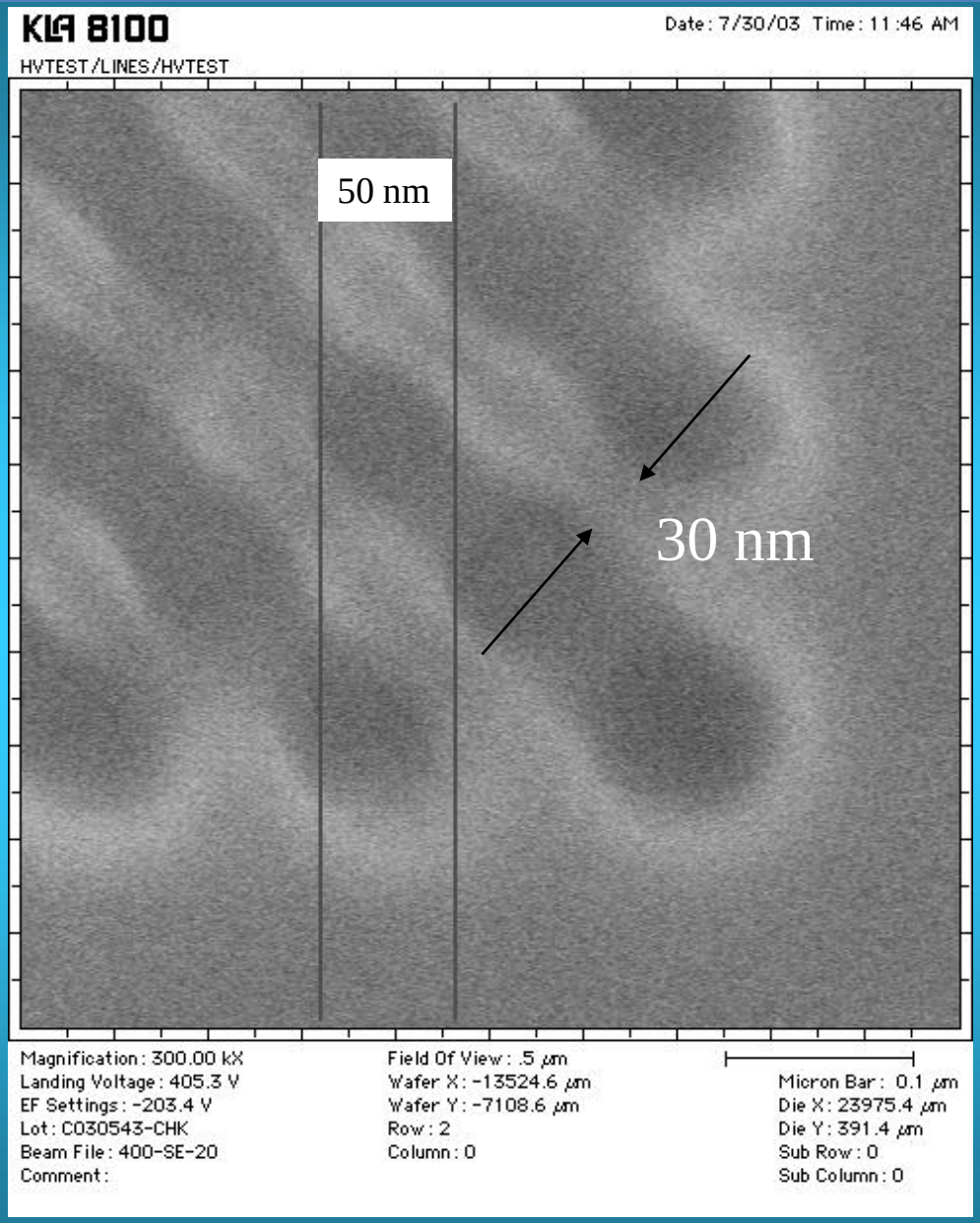

Experimental results DOE for XRM

From the report
DOE Experiment
O. Dhez and M.Salom´e

Experiment performed on ID21 SXM branch, in 16 bunch mode, under vacuum at 6.5keV. The sample used is the PMMA test object.

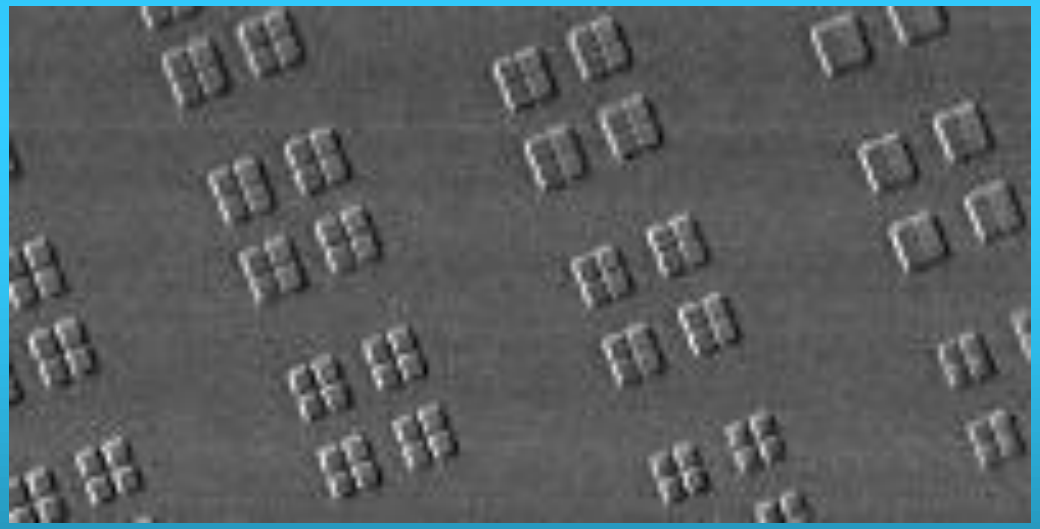

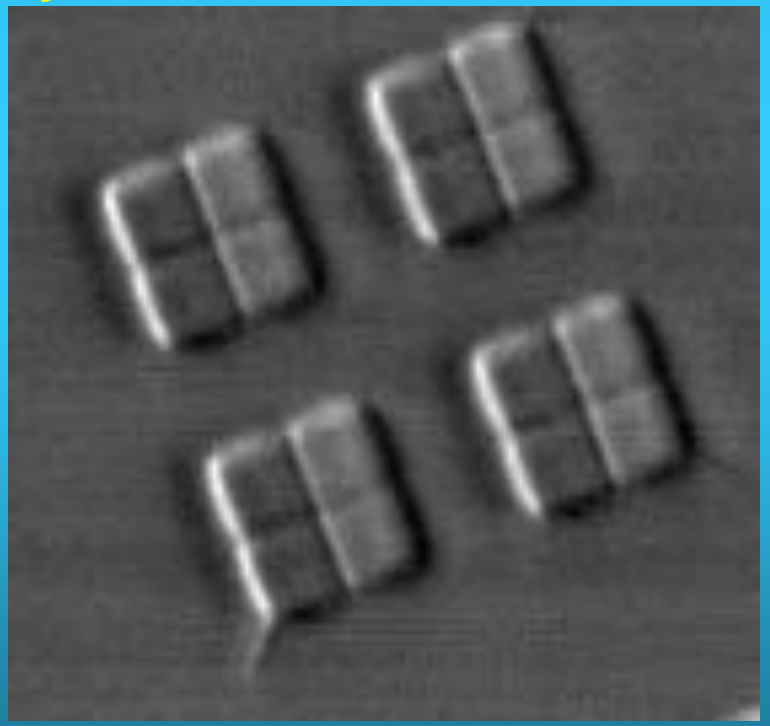

DIC microscopy
On Liver tumoral cells at 7 KeV

Topography

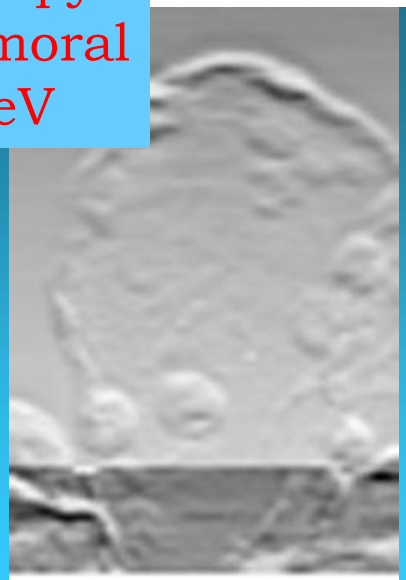

4.8 μm

Chlorine

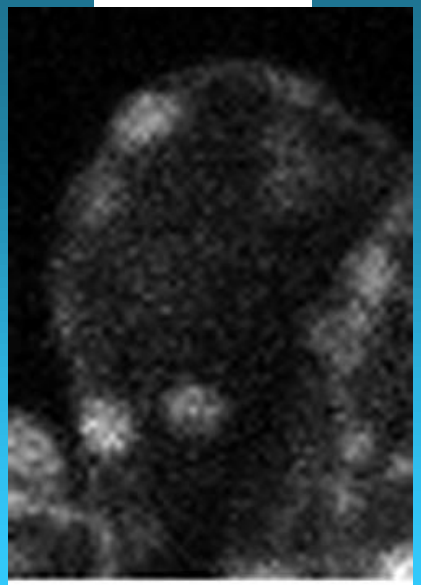

4.8 μm

Phosphorus

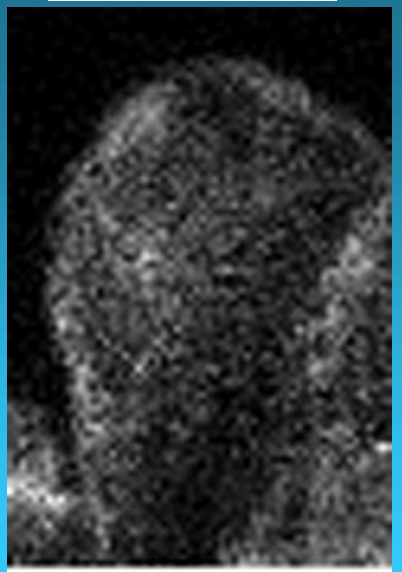

4.8 μm

Potassium

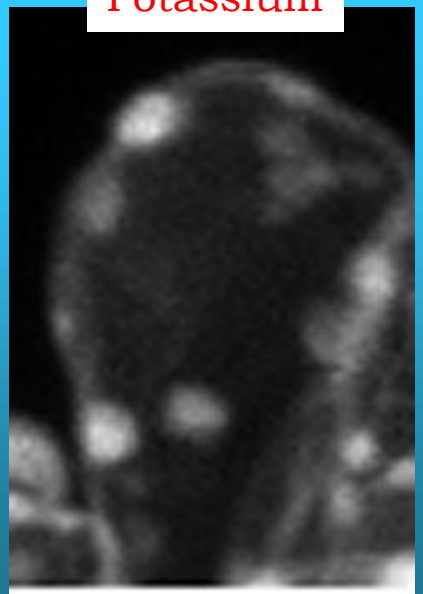

4.8 μm

K&P

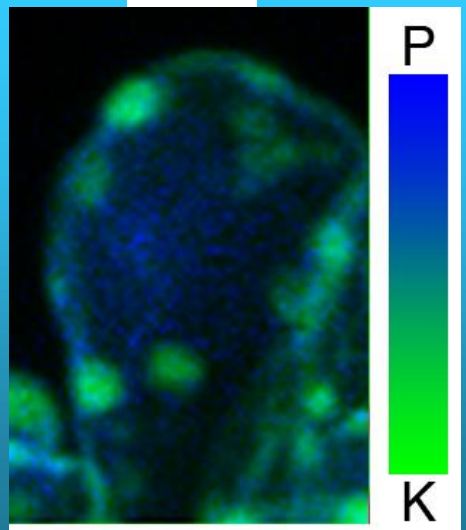

4.8 μm

Scandium

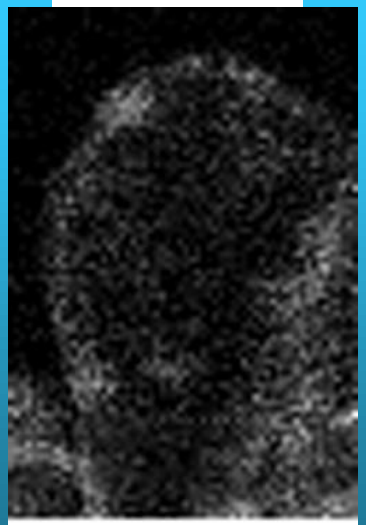

4.8 μm

Sulfur

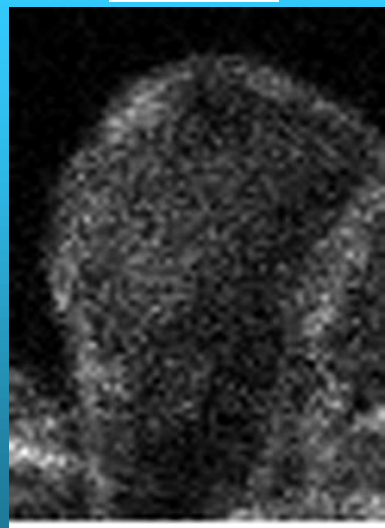

4.8 μm

SAXS experiments

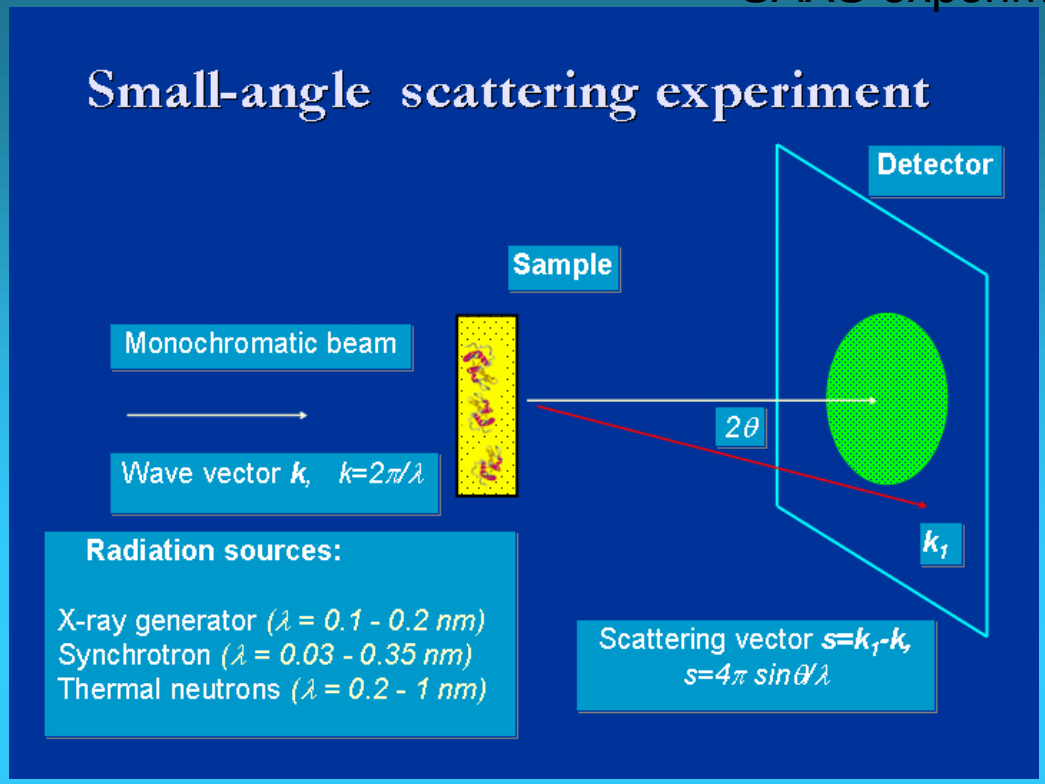

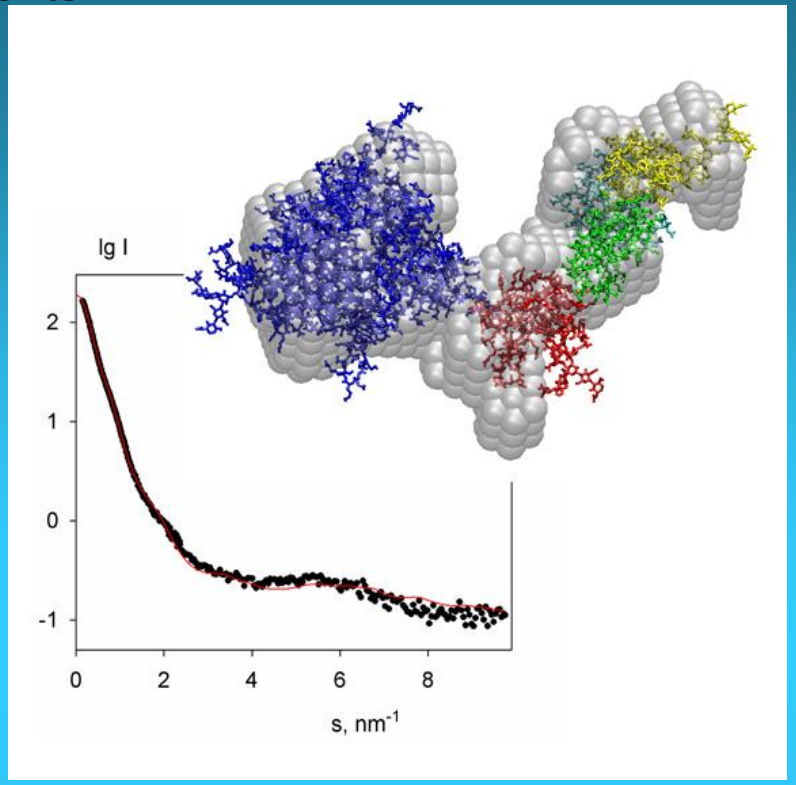

SAXS beamline-Elettra

Using the precise scattering patterns recorded at synchrotrons, SAXS can reveal the shapes of protein molecules and nanoparticles. The X-ray scattering curve on the left (intensity versus scattering angle) was used to create a low-resolution model of a protein, shown in grey. Superimposed on this (in colour) are atomic models of separate domains obtained from crystallography and positioned to fit the SAXS data.

The protein molecule is about 10 nm across. This example illustrates how SAXS can help to assemble together high resolution models of individual domains provided by protein crystallography into the model of the entire macromolecular complex.

Lysozyme fibrillation induced by convective flow under quasi contact-free conditions

A. Accardo et al Soft Matter June 2011

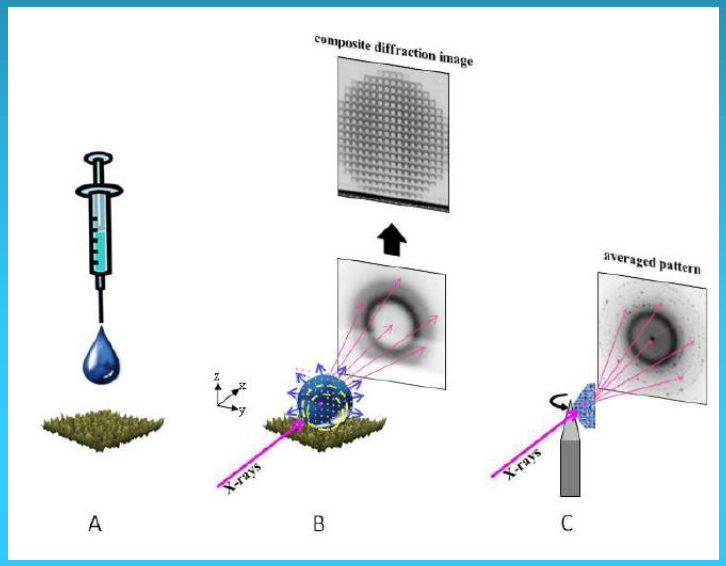

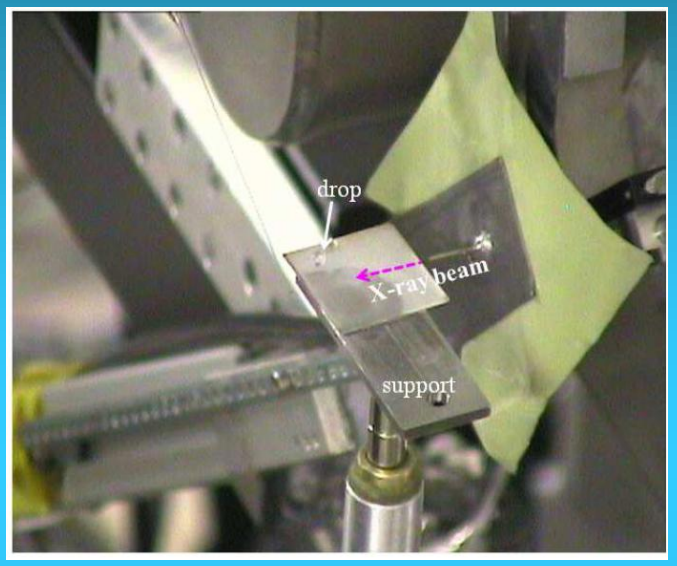

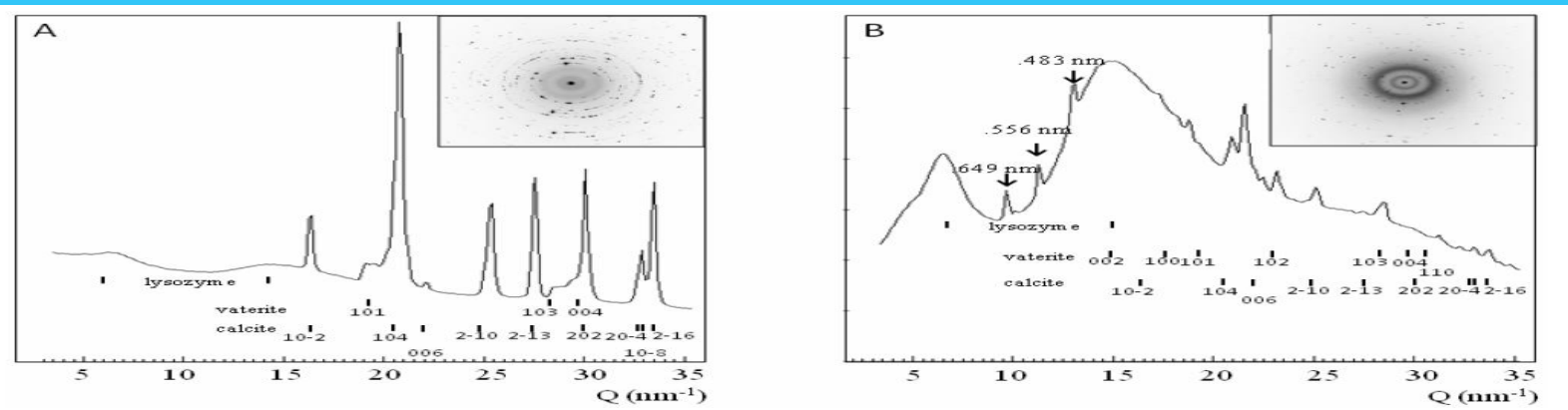

Fig. S5 A: Intensity profile of diffraction pattern from the edge of a 10 mg/ml lysozyme residue. **B**: Intensity profile of diffraction pattern from the edge of a 50 mg/ml lysozyme residue. Miller's indices for the calcite and vaterite unit cells are indicated. The d-spacings of 3 reflections due to an unknown phase are indicated.

Coherent lensless X-ray imaging

H.N. Chapman et al. nature photonics | VOL 4 | DECEMBER 2010 | www.nature.com/naturephotonics

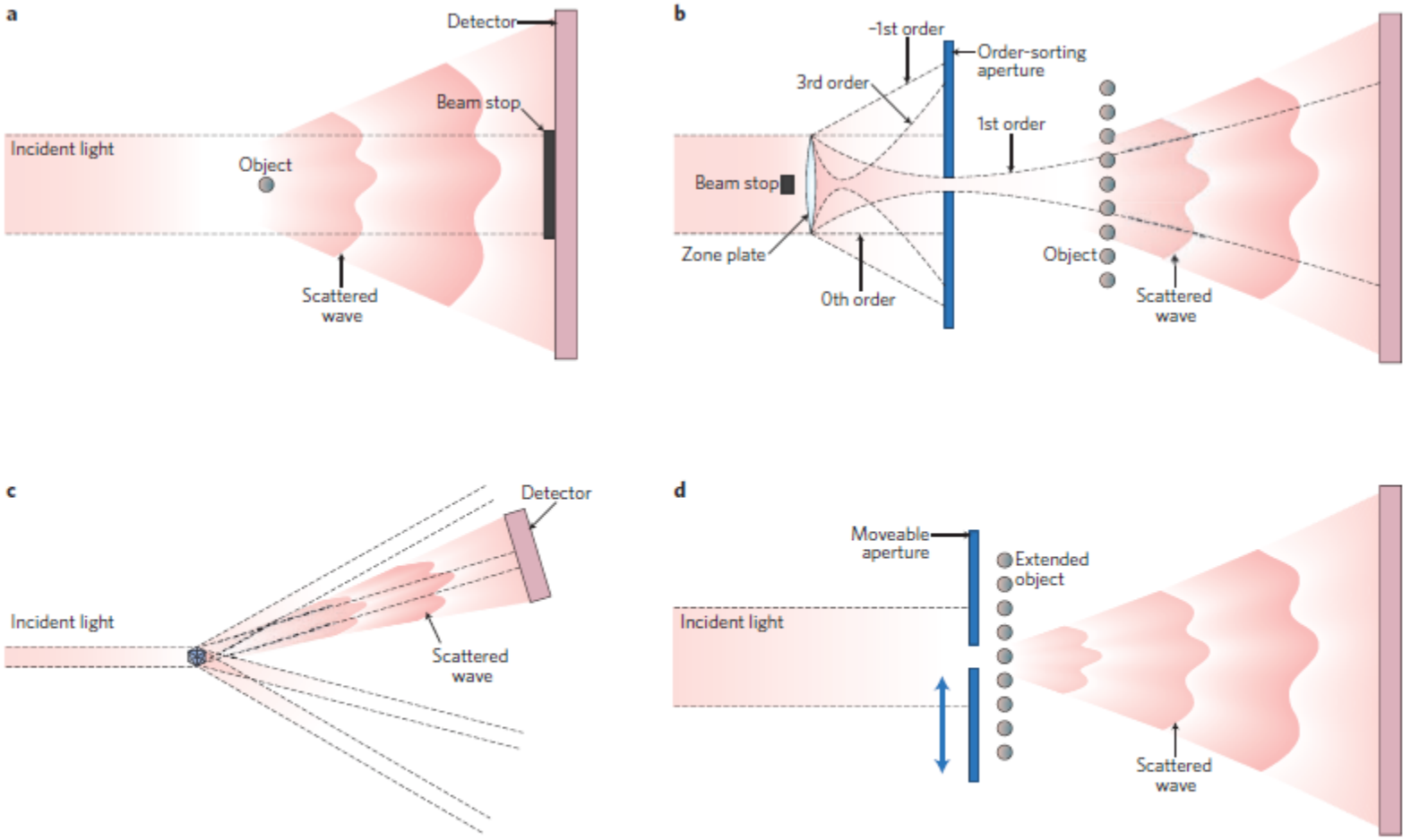

Figure 1 | Experimental configurations for X-ray coherent diffractive imaging. a, Plane-wave CDI, in which a coherent planar beam of X-rays is incident on the sample. **b**, Fresnel CDI, in which a coherent phase-curved beam created by a Fresnel zone plate is incident on the sample. An order-sorting aperture eliminates the unwanted diffracted orders. A beam stop prevents the undiffracted order from passing through the order-sorting aperature. **c**, Bragg CDI, in which a nanocrystal is illuminated and the detailed structure in the Bragg diffraction spots is used to recover information about the shape and strain distribution within the crystal. **d**, Scanning diffraction microscopy, in which a finite beam probe is scanned across the sample and the diffraction pattern observed at each beam position. The finite probe may be formed using a focusing optic such as a Fresnel zone plate.

Biological and material science Imaging

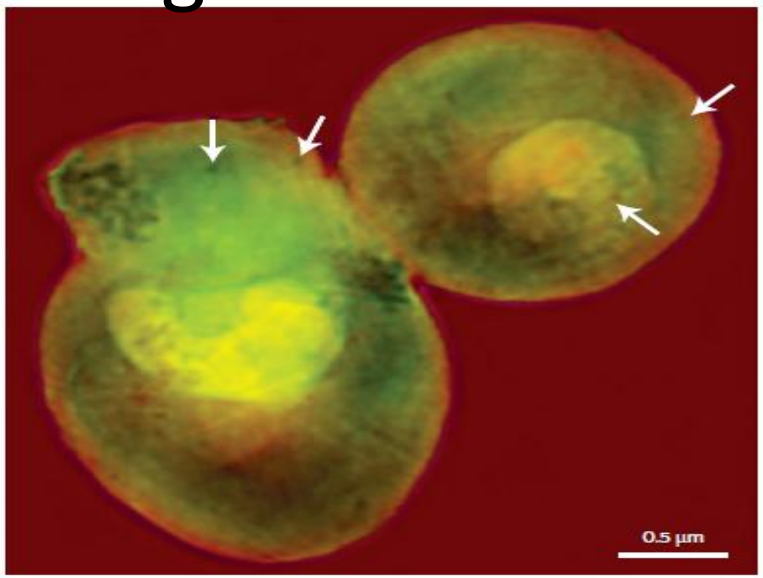

Figure 2 | Biological imaging is an important area for applications of CDI. Optical soft-X-ray image of a yeast cell. The reconstructed complex wave is represented using brightness for magnitude and hue for phase. The arrows indicate the location of immunogold labels. Figure reproduced with permission from ref. 30, © 2010 PNAS.

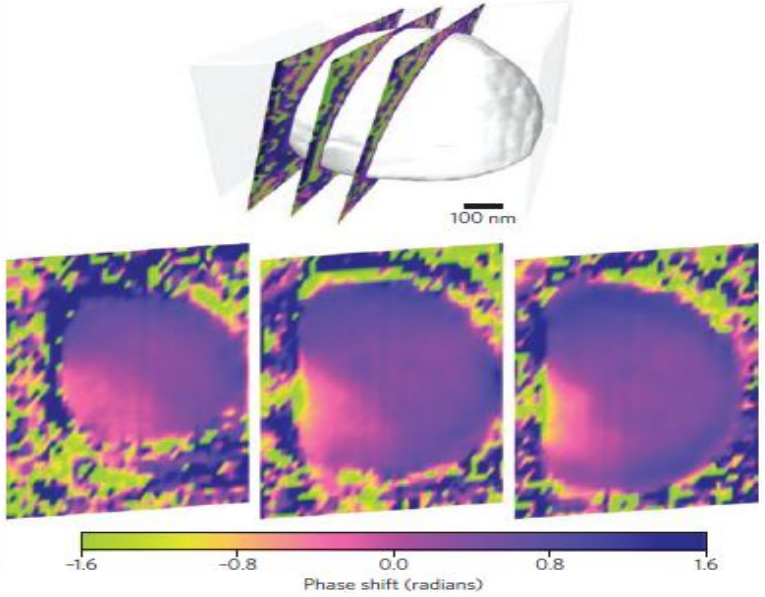

Figure 3 | Bragg CDI is able to recover the three-dimensional shape and strain structure from a nanocrystal. The shape of a gold nanocrystal and the distribution of the phase shift produced by the strain field from within the nanocrystal are shown. Figure reproduced with permission from ref. 45, © 2006 NPG.

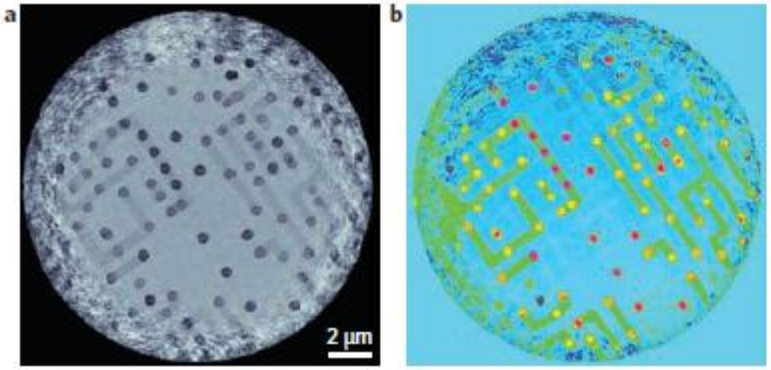

Figure 4 | Scanning diffraction microscopy is able to recover images of extended objects. a,b, Amplitude (**a**) and phase (**b**) distribution of an integrated circuit sample used as a test object. The form of the illuminating probe can also be recovered during the iterative image reconstruction scheme. The pixel size is 36 nm and the sample is 200 µm thick. The X-ray energy used was 7.11 keV. Images courtesy of Pierre Thibault from the Technical University of Munich, Germany.

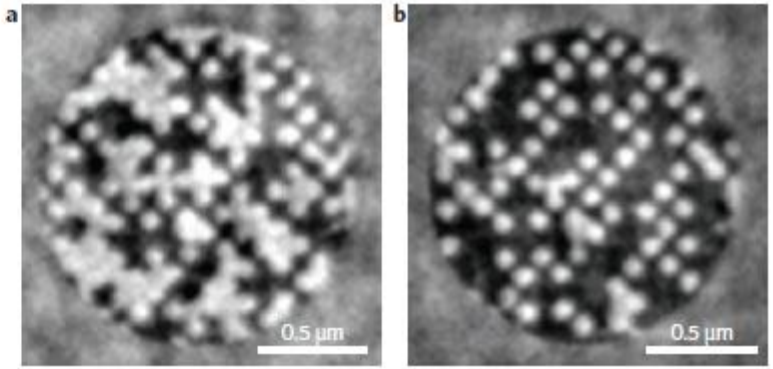

Figure 5 | Holographic reconstructions of a sample containing bit-patterned magnetic media. a,b, The bits consist of a substrate with 80 nm × 80 nm elevated squares in a 120 nm pitch array, coated with a magnetic multilayer film $[Co(5.5\ Å)/Pd(9\ Å)]_{24}$ plus seed and cap layers. The black/white contrast is based on X-ray circular dichroism and corresponds to the local magnetization in the magnetic film pointing up/

Scheme of a typical synchrotron X-ray lithography system

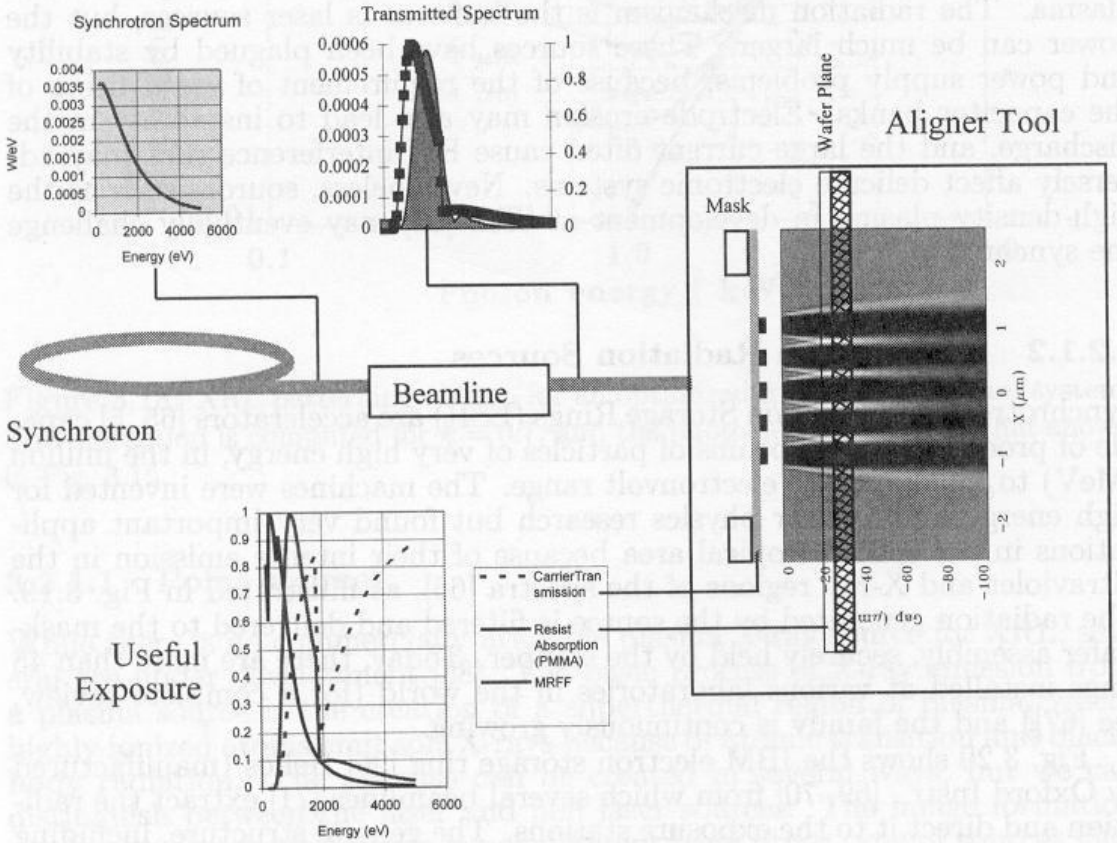

Figure 3.19: Schematic of an X-ray Lithography system based on a synchrotron. Notice the synchrotron, beamline and mask arrangement as well as the changes in the spectrum of the radiation.

Lilit-group

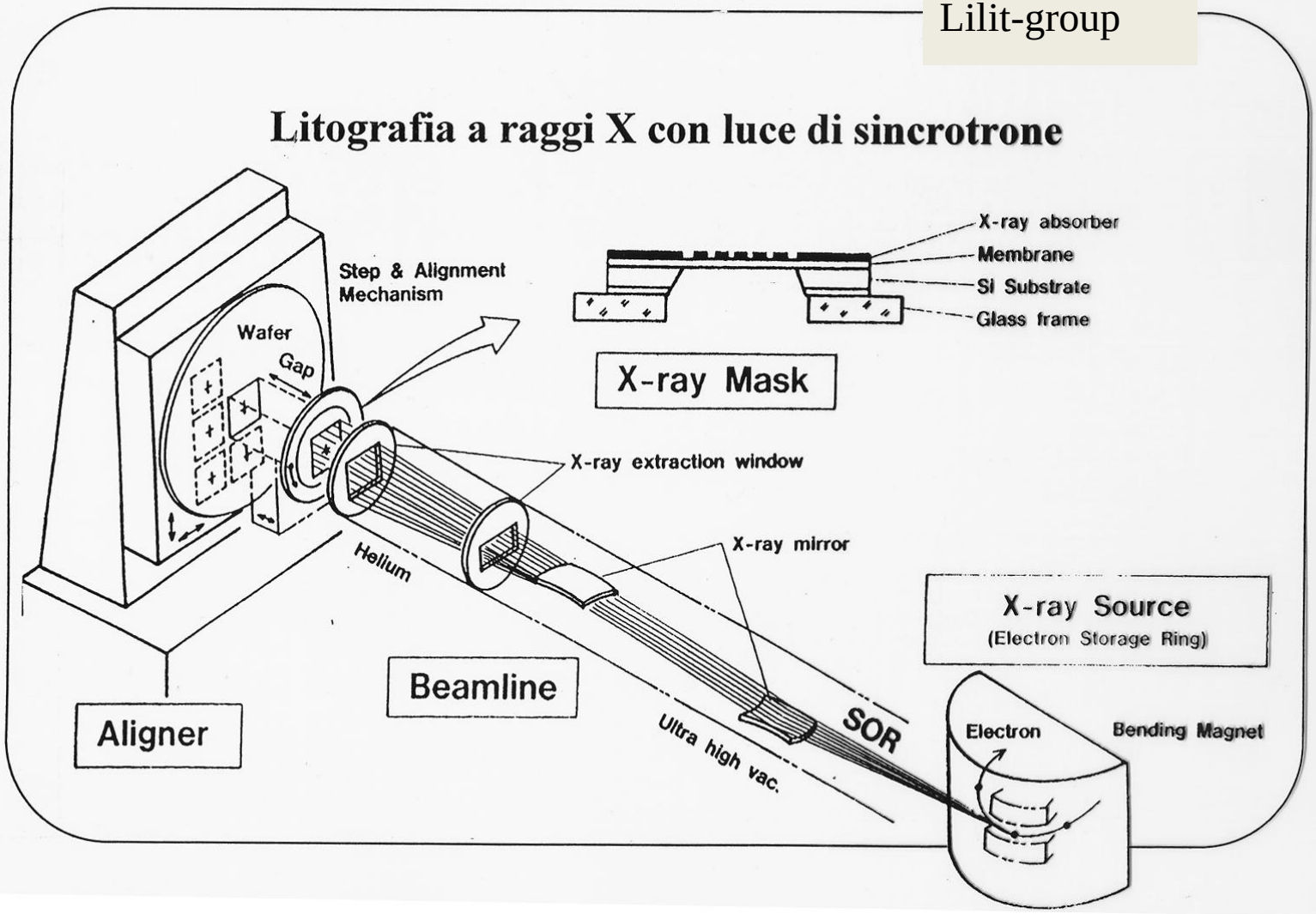
Litografia a raggi X con luce di sincrotrone
X-ray absorber
Membrane
Si Substrate
Glass frame
Step & Alignment Mechanism
Wafer
Gap
X-ray Mask
X-ray extraction window
X-ray mirror
Helium
X-ray Source
(Electron Storage Ring)
Beamline
Aligner
SOR
Ultra high vac.
Electron
Bending Magnet

The beamline in real life

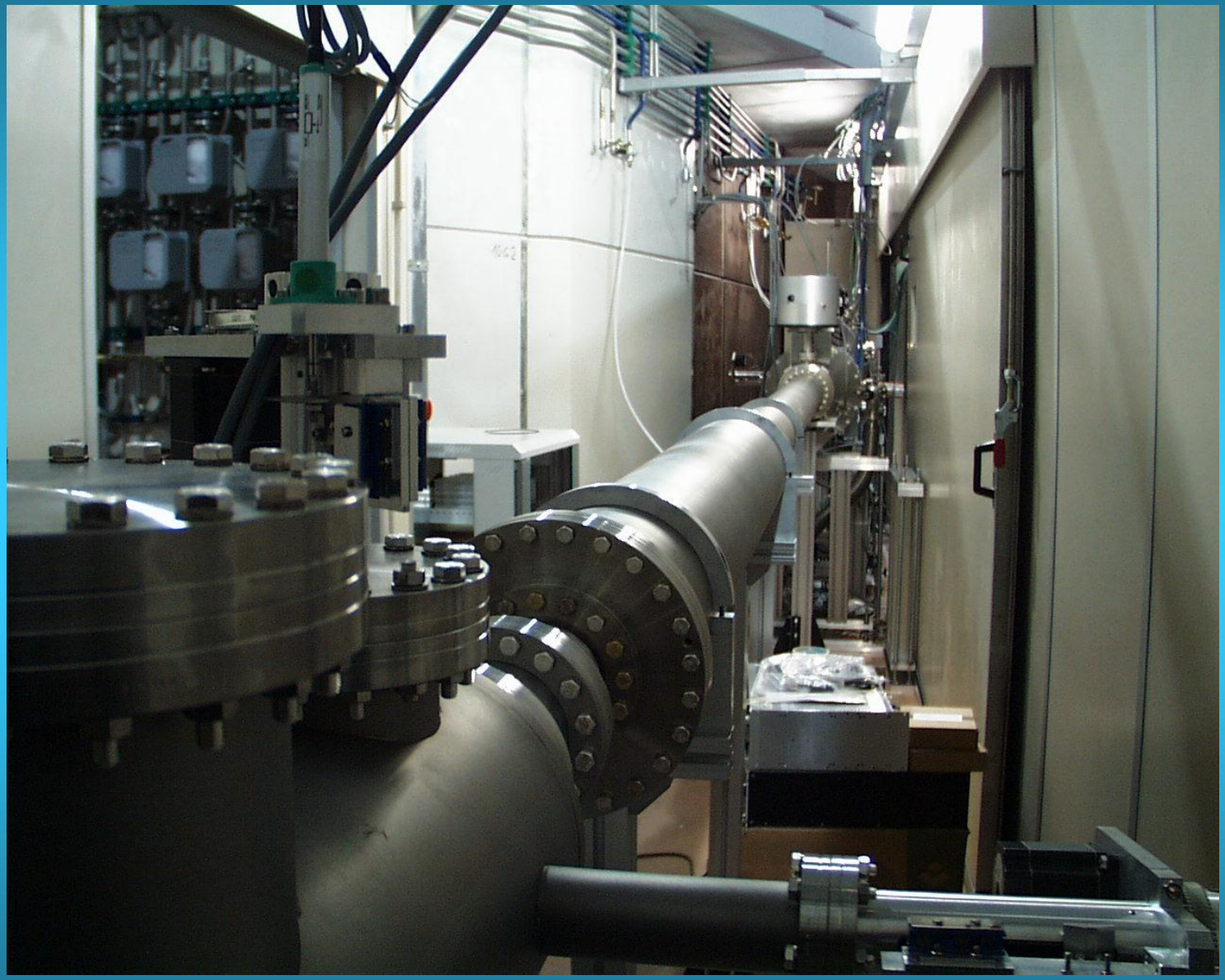

3D PH. Crys. By X-ray litho

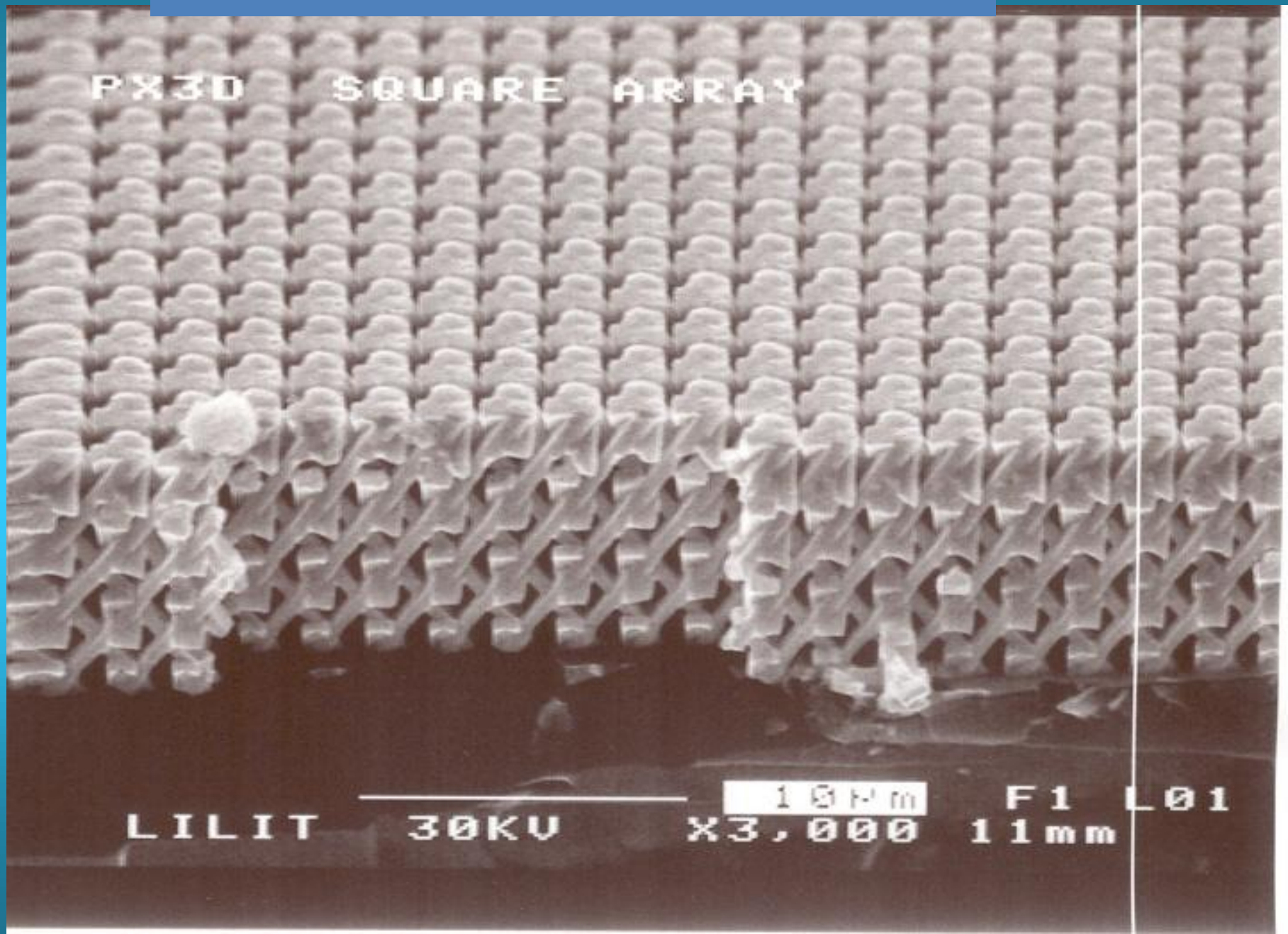

The LIGA process @ Elettra-Trieste

(Lithography, Electroforming, Moulding)

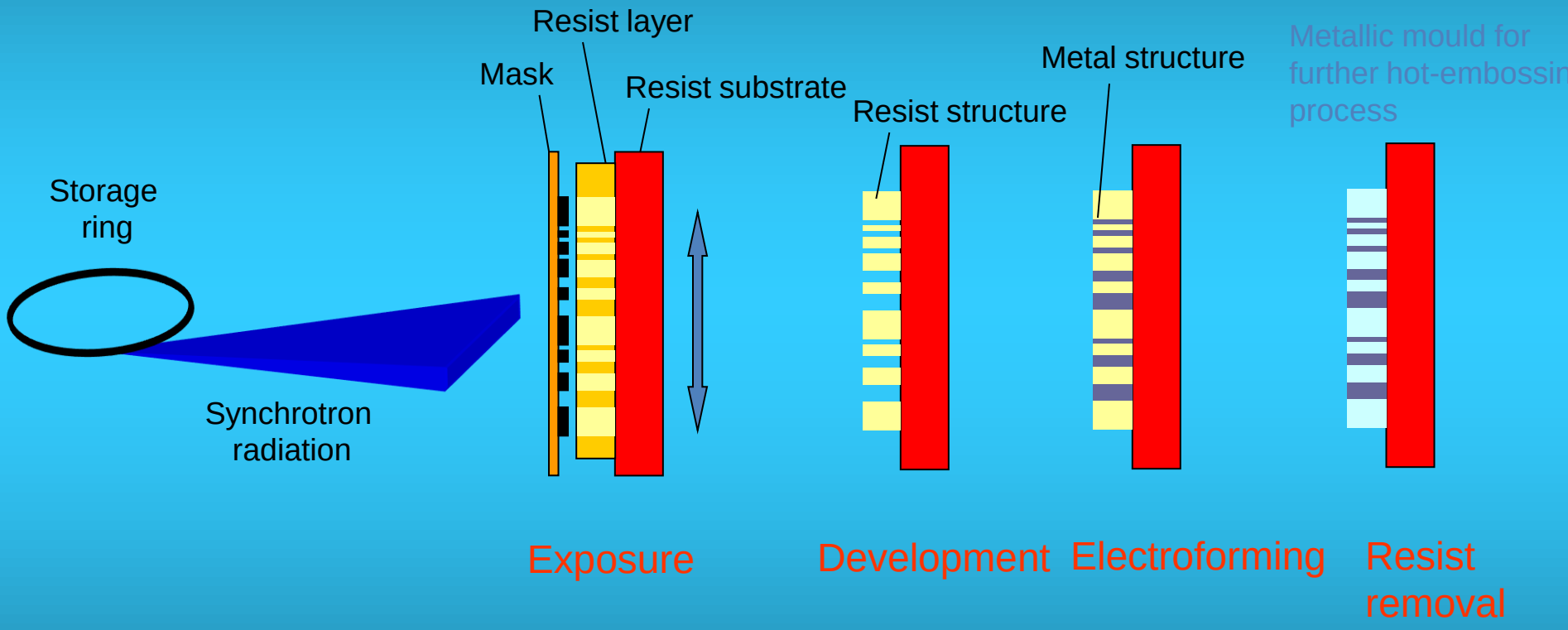

Deep X-Ray Lithography Scanner

Instrumentation @ Elettra

Scanning stage

Example of Copper electroplated test structures

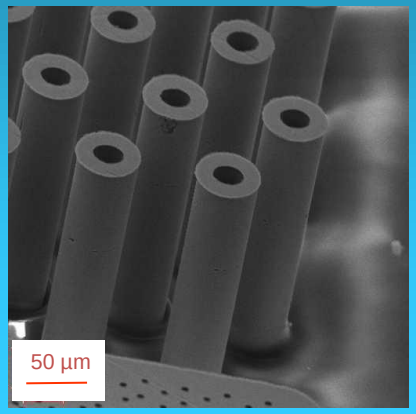

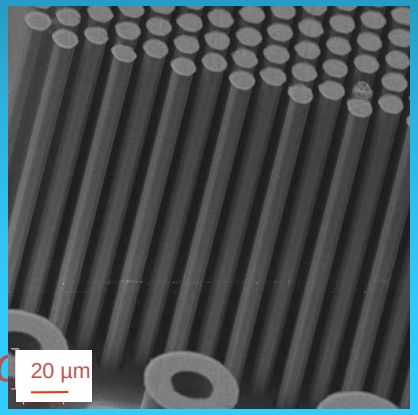

Special features of the LIGA process

Freedom in lateral shaping

Structure heights up to 2-3 mm

High aspect ratio (height/lateral dimensio

Roughness of side walls < 30 nm

Choice of material

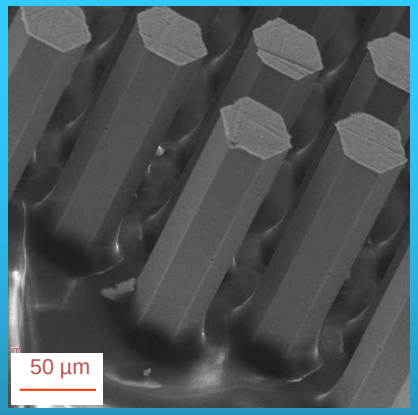

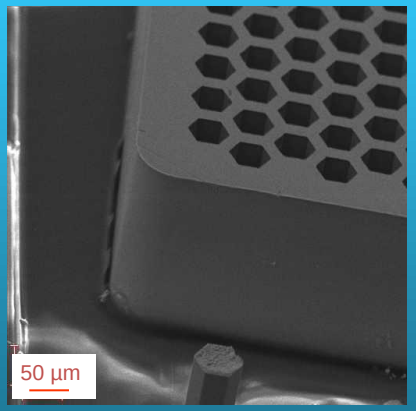

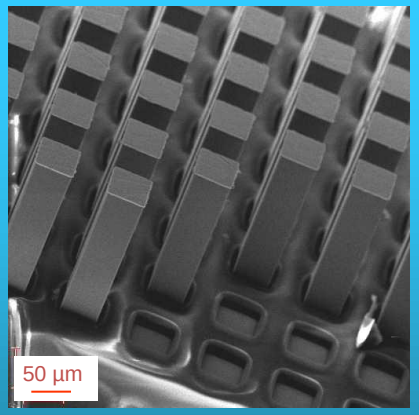

Experimental results: trapping beads

(C. Liberale et al Nature Photonics 2007)

The trapping effectiveness has been tested by depositing on a cover-slip a water suspension of polystyrene spheres having a diameter of 10 µm. The probe-end was immersed in the suspension and was viewed through a standard microscope (10 ×- or 20 ×- objective):

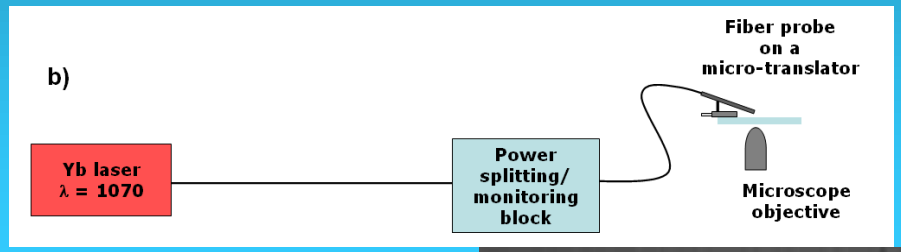

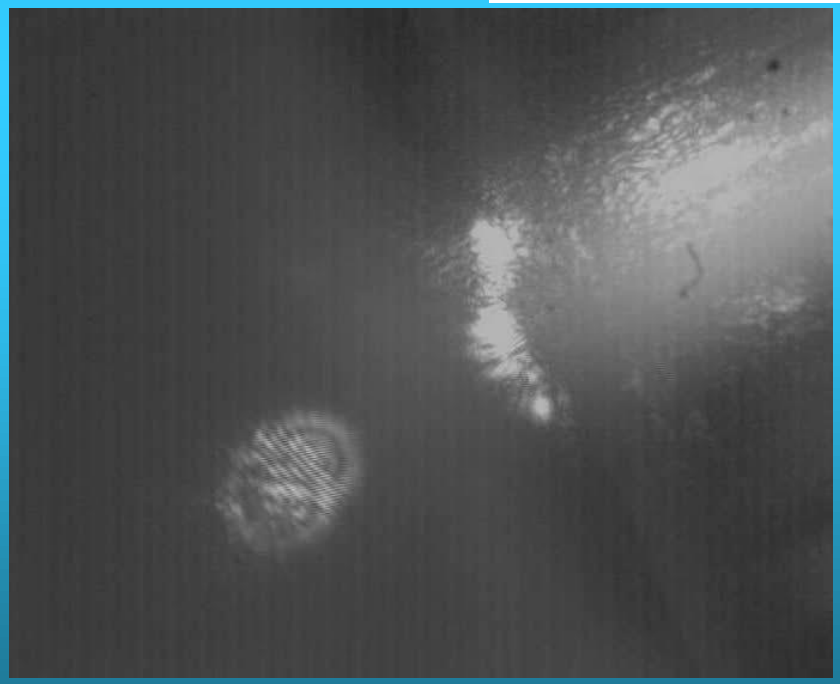

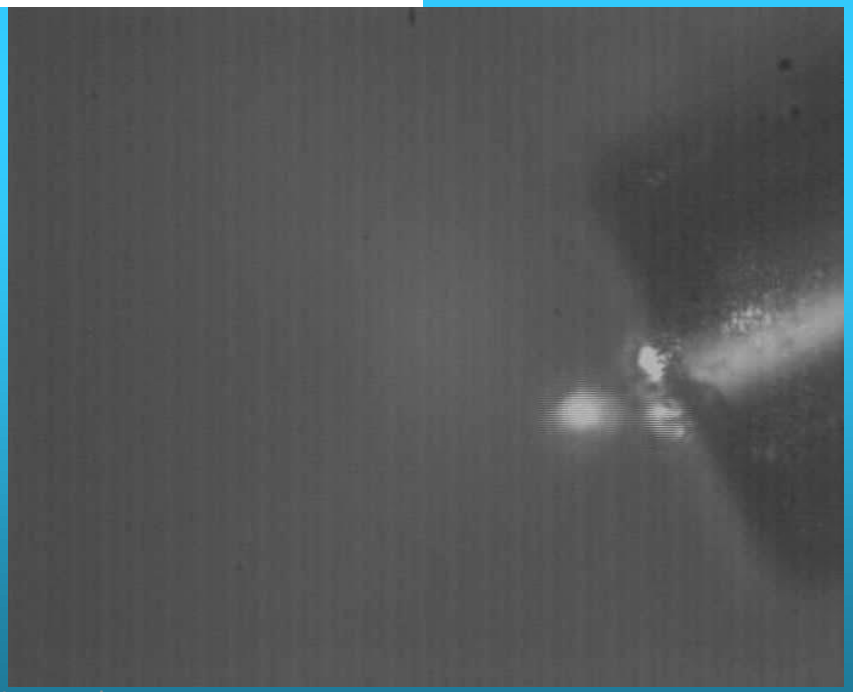

Conclusions

IIT beamlines of interest

1. **High resolution Microscopy: Phase contrast and Differential Interference Contrast DIC technique.**
2. **Coherent lensless imaging**
3. **SAXS-WAXS for the structure of macromolecule "in solution"**
4. **Combination of X-ray microscopy with novel manipulation techniques., ex Optical Tweezers, super hydrophobic microfluidics etc.**
5. **Lithography beamlines from bending magnet**
6. **Thz microscopy combined with nanoantennas**

Acknowledgments

- IIT Nanostructures department
- University of Magna Graecia Cz Italy
- Elettra & TASC-Trieste
- ESRF-Grenoble